Antibodies from a human survivor define sites of vulnerability for broad protection against ebolaviruses

Anna Z. Wec,[1,10] Andrew S. Herbert,[2,10] Charles D. Murin,[3,4] Elisabeth K. Nyakatura,[5] Dafna M. Abelson,[6] J. Maximilian Fels,[1] Shihua He,[7,8] Rebekah M. James,[2] Marc-Antoine de La Vega,[7,8] Russell R. Bakken,[2] Eileen Goodwin,[9] Hannah L. Turner,[3] Rohit K. Jangra,[1] Larry Zeitlin,[6] Xiangguo Qiu,[7,8] Jonathan R. Lai,[5] Laura M. Walker,[9] Andrew B. Ward,[3] John M. Dye,[2,*] Kartik Chandran,[1,*] and Zachary A. Bornholdt[6,11*]

[1]Department of Microbiology and Immunology, Albert Einstein College of Medicine, Bronx, NY 10461, USA

[2]U.S. Army Medical Research Institute of Infectious Diseases, Fort Detrick, MD 21702, USA

[3]Department of Integrative Structural and Computational Biology, The Scripps Research Institute, La Jolla, California 92037, USA

[4]Department of Immunology and Microbial Science, The Scripps Research Institute, La Jolla, California 92037, USA

[5]Department of Biochemistry, Albert Einstein College of Medicine, Bronx, NY 10461, USA

[6]Mapp Biopharmaceutical Inc., San Diego, CA 92121, USA

[7]Special Pathogens Program, National Microbiology Laboratory, Public Health Agency of Canada, Winnipeg, Manitoba R3E 3R2, Canada

[8]Department of Medical Microbiology, University of Manitoba, Winnipeg, Manitoba, R3E 0J9, Canada

[9]Adimab, LLC, Lebanon, NH 03766, USA

[10]Co-first authors

[11]Lead contact

[*]To whom correspondence should be addressed. Email: zachary.bornholdt@mappbio.com, kartik.chandran@einstein.yu.edu, john.m.dye1.civ@mail.mil. Twitter: @chandranlab.

SUMMARY

Experimental monoclonal antibody (mAb) therapies have shown promise for treatment of lethal Ebola virus (EBOV) infections, but their species-specific recognition of the viral glycoprotein (GP) has limited their use against other divergent ebolaviruses associated with human disease. Here, we mined the human immune response to natural EBOV infection, and identified mAbs with exceptionally potent pan-ebolavirus neutralizing activity, and protective efficacy against three virulent ebolaviruses. These mAbs recognize an inter-protomer epitope in the GP fusion loop, a critical and conserved element of the viral membrane fusion machinery, and neutralize viral entry by targeting a proteolytically primed, fusion-competent GP intermediate (GP_{CL}) generated in host cell endosomes. Only a few somatic hypermutations are required for broad antiviral activity, and germline-approximating variants display enhanced GP_{CL} recognition, suggesting that such antibodies could be elicited more efficiently with suitably optimized GP immunogens. Our findings inform the development of both broadly effective immunotherapeutics and vaccines against filoviruses.

INTRODUCTION

Viruses of the family *Filoviridae* (filoviruses) cause outbreaks of a lethal disease for which no FDA-approved treatments or vaccines are available. The unprecedented 2013–2016 Ebola virus (EBOV) epidemic in Western Africa highlighted the potential of these agents to cause health emergencies of international scope, and has accelerated the development of vaccines and countermeasures (de La Vega et al., 2015; Kuhn et al., 2014). At the height of this epidemic, several early-stage therapeutics and vaccines were evaluated under compassionate use protocols (Wong and Kobinger, 2015). Arguably the most successful of these is ZMapp™, an immunotherapeutic comprising three mouse/human chimeric monoclonal antibodies (mAbs), c2G4, c4G7, and c13C6, which target and neutralize the trimeric glycoprotein (GP) spikes on the surface of viral particles. ZMapp was highly effective at reversing advanced disease caused by EBOV in non-human primates (NHPs), and provided initial evidence of protective efficacy in a Phase II clinical trial (Group and Multi-National, 2016; Qiu et al., 2014). Despite its promise, ZMapp suffers from a key limitation. It lacks activity against other filoviruses associated with human disease, including Bundibugyo virus (BDBV), Sudan virus (SUDV), and Marburg virus (MARV), because its component mAbs are specific for EBOV GP and do not recognize and neutralize these divergent GP proteins (Murin et al., 2014). The public health threat represented by BDBV and SUDV in particular, which caused ≈40% of all ebolavirus infections prior to 2013 (Burk et al., 2016), and the unknown risk posed by any newly emerging or engineered ebolaviruses, demands an urgent response.

Given the scientific and logistical hurdles inherent in developing a separate mAb therapeutic for each filovirus, recent work has focused on the development of broadly protective anti-filovirus immunotherapies. Frei and co-workers (2016) combined known EBOV and SUDV GP-specific neutralizing antibodies (NAbs) KZ52 and F4 (a humanized variant of 16F6), respectively, to generate bispecific antibodies that protected against both viruses in mice. More recently, bispecific antibodies combining two broadly reactive but non-neutralizing mAb specificities targeting virus-host receptor interactions were shown to neutralize all known ebolaviruses through a “Trojan horse” mechanism, and to protect mice from challenge with EBOV and SUDV (Wec et al., 2016). The presence of cross-reactive and cross-neutralizing antibodies in natural antibody repertoires elicited by monospecific ebolavirus infection or immunization has also been noted (Bornholdt et al., 2016; Macneil et al., 2011; Natesan et al., 2016; Ou et al., 2012), and antibody discovery efforts have yielded cross-neutralizing mAbs with increased protective breadth. Flyak and co-workers (2016) isolated mAbs from a human survivor of BDBV infection, and identified several that neutralized EBOV, BDBV, and SUDV. Complex vaccination strategies in NHPs or mice have afforded the discovery of mAbs that neutralize both EBOV and SUDV (Furuyama et al., 2016; Howell et al., 2016; Keck et

al., 2015). To date, however, these efforts have uncovered only a single canonical IgG molecule—the mouse mAb 6D6—with true pan-ebolavirus neutralizing activity (Furuyama et al., 2016). Moreover, no natural or engineered antibody has yet been shown to protect animals against the three known virulent ebolaviruses, EBOV, BDBV, and SUDV (Burk et al., 2016).

Here, we sought to perform a systematic analysis of the breadth of the anti-ebolavirus neutralizing mAb response in humans. Accordingly, we screened our recently published collection of 349 mAbs isolated from a human survivor of the 2013–2016 West African EBOV outbreak (Bornholdt et al., 2016) for mAbs capable of neutralizing EBOV, BDBV, and SUDV. We identified two mAbs that could potently neutralize all five ebolaviruses and confer post-exposure protection against EBOV, BDBV, and SUDV in small-animal models of ebolavirus challenge. Follow-up studies indicated that these mAbs recognize, with picomolar affinity, a hitherto unknown GP epitope that encompasses membrane-seeking residues in the internal fusion loop and a highly conserved essential glycan, and mediate neutralization via a novel mechanism that targets a proteolytically cleaved GP intermediate deep in the endocytic pathway. Taken together, our findings inform the development of pan-ebolavirus and pan-filovirus immunotherapeutics, and the design of filovirus subunit vaccines tailored to elicit the same types of highly potent cross-protective antibodies.

RESULTS

Identification of cross-reactive and cross-neutralizing mAbs

To identify mAbs in the Ebola virus disease survivor library that could cross-react with GP proteins from other ebolaviruses, we screened recombinant VSV (rVSV) particles displaying prototypic GP proteins from EBOV, BDBV, and SUDV by ELISA. We found that 72% of the mAbs were also able to recognize BDBV GP, whereas only 11% demonstrated significant cross-reactivity to SUDV GP (Figure S1A), consistent with the degree of amino acid sequence conservation among these glycoproteins. 37 of 349 mAbs reacted with all three ebolavirus glycoproteins by ELISA (Figure S1B). Within this subset, 16 mAbs belonged to the glycan cap epitope group (c13C6 competitors), 10 mAbs targeted the GP base (KZ52 competitors), another 10 were directed against the α–helical heptad repeat 2 sequence in the GP2 “stalk” (HR2 epitope group, ADI-15974 competitors), and one mAb belonged to an unassigned/unknown GP1-specific epitope group (Bornholdt et al., 2016).

We next assayed the 37 cross-reactive mAbs for their capacity to inhibit infection by rVSV particles bearing SUDV GP, the most divergent from EBOV GP in amino acid sequence. Neutralization potency was initially evaluated at two concentrations, 33 and 330 nM, and mAbs advanced if greater than 50% reduction in infection was observed

Figure 1

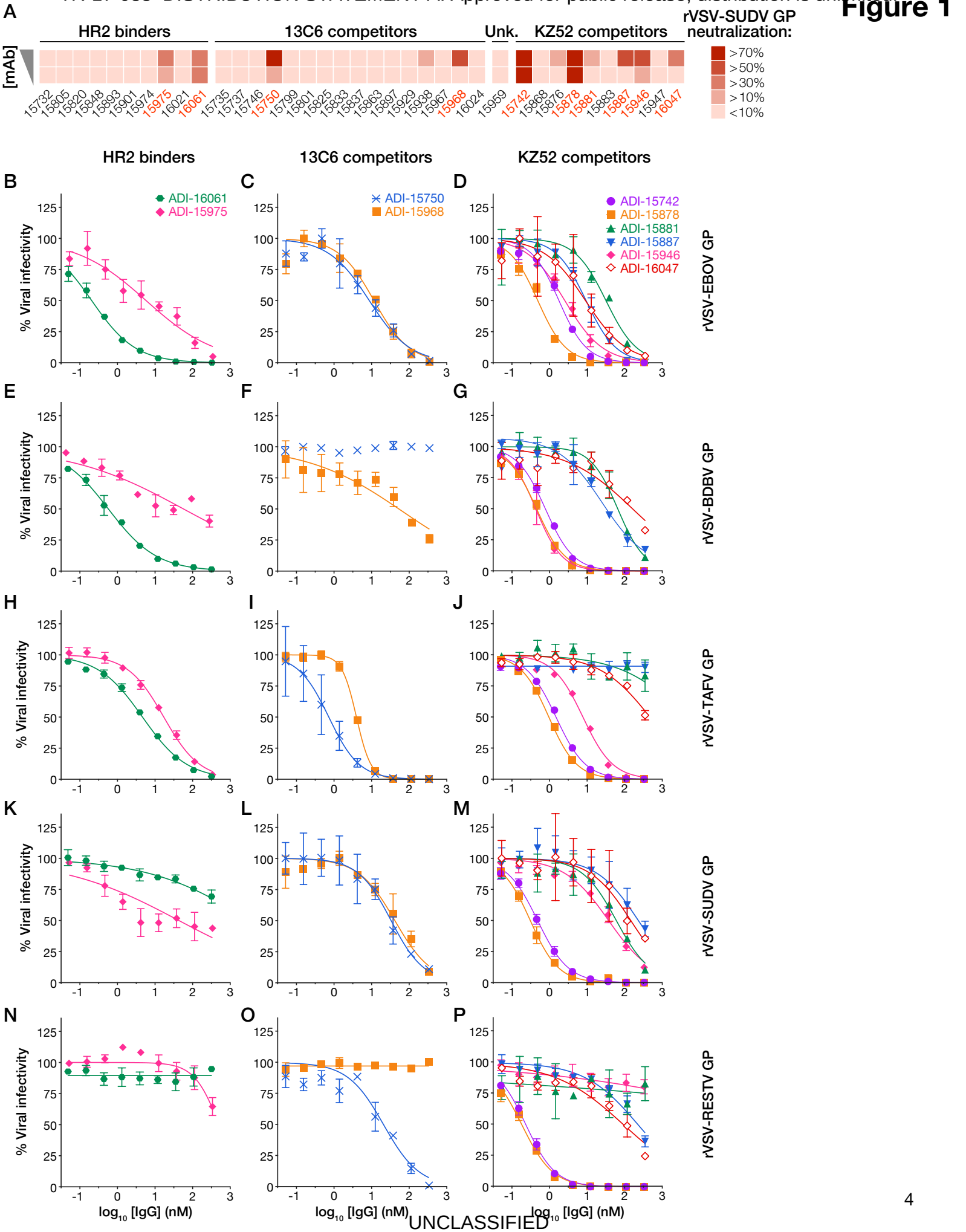
A
HR2 binders
13C6 competitors
Unk.
KZ52 competitors
rVSV-SUDV GP neutralization:
>70%
>50%
>30%
>10%
<10%
[mAb]
15732 15805 15820 15848 15893 15901 15974 15975 16021 16061
15735 15737 15746 15750 15799 15801 15825 15833 15837 15863 15897 15929 15938 15967 15968 16024
15959 15742 15868 15876 15878 15881 15883 15887 15946 15947 16047
HR2 binders
13C6 competitors
KZ52 competitors
B
C
D
ADI-16061
ADI-15975
ADI-15750
ADI-15968
ADI-15742
ADI-15878
ADI-15881
ADI-15887
ADI-15946
ADI-16047
% Viral infectivity
rVSV-EBOV GP
E
F
G
rVSV-BDBV GP
H
I
J
rVSV-TAFV GP
K
L
M
rVSV-SUDV GP
N
O
P
rVSV-RESTV GP
log10 [IgG] (nM)

Figure 1. Identification of broadly neutralizing mAbs from a human survivor of EBOV infection

(A) Heat map of rVSV-SUDV GP neutralization activity by cross-reactive mAbs identified in a screen of 349 mAbs from a human EBOV disease survivor. Activity at two mAb concentrations, 330 nM (top row) and 33 nM (bottom row) is shown. mAbs with neutralizing activity at both concentrations are highlighted in red. See also Figure S1.

(B–P) Dose curves for neutralization of recombinant VSVs bearing ebolavirus glycoproteins by mAbs with SUDV GP-specific neutralizing activity from panel A. TAFV, Taï Forest virus. RESTV, Reston virus. Means±standard deviation (SD) for three replicates are shown. See also Table S1.

at the higher mAb dose (Figure S1C–F). Only 10 of 37 cross-reactive mAbs showed significant neutralizing activity against rVSV-SUDV GP. Six of these neutralizing antibodies (NAbs) were members of the KZ52 competition group and targeted the GP base, whereas the remaining four were equally divided between the HR2 and glycan cap antigenic regions of GP (Figures 1A and S1C–F). These and previous results (Flyak et al., 2016) suggest that a small subset of cross-reactive and cross-neutralizing antibodies is generated by the human immune response in the course of natural ebolavirus infection.

Analysis of pan-ebolavirus neutralizing activity in vitro

To further evaluate the breadth and potency of neutralization by the top 10 NAbs identified in our screen, we performed dose-response neutralization assays with rVSVs bearing GPs from all five known ebolaviruses—EBOV, BDBV, SUDV, RESTV and TAFV (Figures 1B–P and Table S1). The HR2 binder, ADI-16061, potently neutralized infection by rVSVs bearing EBOV, BDBV and TAFV GP, with half-maximal inhibitory concentration (IC_{50}) values below 5 nM, but had little or no activity against those bearing SUDV and RESTV GP. The second NAb from this epitope group, ADI-15975, possessed an even narrower antiviral spectrum, showing strong activity only against rVSV-EBOV GP (Figures 1B, E, H, K, N and Table S1).

The glycan cap binders, ADI-15750 and ADI-15968, neutralized rVSVs bearing EBOV, TAFV and SUDV GP, albeit with weaker activity against SUDV GP (Figures 1C, I, L and Table S1). Further, ADI-15750 was effective at neutralizing rVSV-RESTV GP but not rVSV-BDBV GP, whereas ADI-15968 only weakly inhibited infection with rVSV-BDBV GP and completely failed to neutralize rVSV-RESTV GP (Figures 1F, O, and Table S1). Thus, none of the mAbs directed against the GP stalk or glycan cap structural regions demonstrated pan-ebolavirus neutralizing profiles, consistent with the limited antigenic conservation across those GP surfaces (Figures 4 and S3).

Two NAbs recognizing the GP base, ADI-15878 and ADI-15742, possessed exceptionally broad and potent neutralizing activity (IC_{50}<2 nM) against all five rVSV-GPs (Figures 1D, G, J, M, P and Table S1). A third NAb from this group, ADI-15946, potently neutralized EBOV, BDBV and TAFV, but showed reduced or no activity towards rVSVs bearing SUDV and RESTV GP, respectively (Figures 1 D, G, J, M, P, and Table S1). The remaining three NAbs in this epitope class demonstrated narrower and less potent neutralization profiles, and were not pursued further.

We advanced the broadest and most potent neutralizers in each epitope group—ADI-16061, ADI-15750, ADI-15878, ADI-15742, and ADI-15946—for testing against authentic EBOV, BDBV and SUDV (Figure 2). The results largely corroborated our findings in the rVSV-GP surrogate system, and confirmed that only the base binders ADI-15878 and ADI-15742 could potently neutralize infection by all three viruses ($IC_{50} \leq 1$ nM) (Fig-

Figure 2

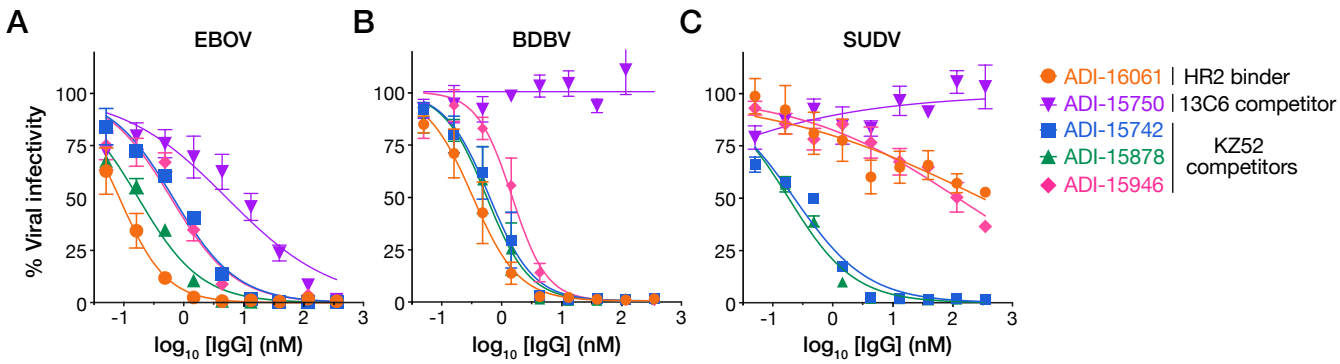
A
EBOV
B
BDBV
C
SUDV
% Viral infectivity
100
75
50
25
0
-1
0
1
2
3
log10 [IgG] (nM)
ADI-16061 | HR2 binder
ADI-15750 | 13C6 competitor
ADI-15742
ADI-15878
ADI-15946
KZ52 competitors

Figure 2. Potency and breadth of authentic ebolavirus neutralization by human NAbs

(A–C) Dose curves for neutralization of authentic EBOV (A), BDBV (B), and SUDV (C) by top NAbs identified in Figure 1. Means±SD for three replicates are shown. See also Table S2.

ure 2 and Table S2). However, the activity of these NAbs did not extend to the more divergent filovirus GPs of Lloviu virus (LLOV) and Marburg virus (MARV) (Table S1). Together, these findings underscore the challenges inherent in achieving pan-filovirus, or even pan-ebolavirus neutralization with single mAbs targeting surface-exposed GP epitopes.

Mapping of cross-neutralizing epitopes using negative-stain electron microscopy and escape mutant analysis

To visualize each GP-NAb complex, we performed negative-stain transmission electron microscopy (EM) studies of the fragments antigen binding (Fabs) of ADI-16061, ADI-15750, ADI-15878, ADI-15742, and ADI-15946 bound to trimeric soluble EBOV GP (GPΔTM). 3D reconstructions determined from the EM class averages confirmed previous epitope group assignments, which were made on the basis of competitive binding experiments (Bornholdt et al., 2016). To identify putative NAb-contacting residues in GP, we fit the recently solved unliganded EBOV GPΔMuc X-ray crystal structure [PDB ID: 5JQ3; (Zhao et al., 2016)] into the GP envelope obtained by image reconstruction (Figure 3). Further, to identify GP residues important for NAb binding and viral neutralization, we selected neutralization escape mutants (Figures 3, S2–S3). rVSV-GPs were serially passaged in the presence of each NAb until complete resistance to neutralization was observed, and the *GP* genes of resistant viral clones were sequenced to identify escape mutations (Figures 3, S2–S3).

ADI-16061 bound to HR2 and an N–terminal portion of the membrane proximal external region (MPER) between residues 621–640 in the GP2 stalk, with an angle of approach perpendicular to the GP stalk and parallel to the viral membrane (Figure 3A). Despite the compact nature of the GP stalk, three Fabs could bind per GP trimer, each rotated by about 50˚ with respect to the threefold symmetry axis of the GP spike. Two independent mutations in HR2, H628N and D632E (Figure 3E), greatly reduced GP-NAb binding (Figure S2A), and afforded escape from viral neutralization (Figure S2B). While the escape mutation H628N can be visualized in the EBOV GP X-ray crystal structure (Zhao et al., 2016), the complete ADI-16061 epitope likely extends past the last resolved amino acid residue (631), inclusive of D632E, and into the MPER (EBOV GP residues ≈633–657) (Regula et al., 2013). The high degree of viral species-dependent sequence variation in the MPER probably accounts for the failure of ADI-16061 to neutralize RESTV and SUDV (Figures 1–2 and S3A).

Complexes between ADI-15750, the sole glycan cap binder with broad neutralizing potential, and GPΔTM, were not amenable to 3D reconstruction because only partial mAb occupancy was observed, likely as a result of poor binding affinity (data not shown). However, 2D class averages of these complexes revealed that the Fabs engaged GP axially to the viral membrane, reminiscent of the binding mode of ZMapp

component c13C6 and a number of other glycan cap binders (Bornholdt et al., 2016; Murin et al., 2014; Pallesen et al., 2016) (Figure S4A). rVSV-EBOV GP particles escaped ADI-15750 neutralization via mutations at GP residues 231, 247, 254, 271-272, 279 and 283, which compromised GP-NAb binding to varying degrees (Figures S2–S4). The ADI-15750 binding footprint inferred from the escape mutant analysis appears to overlap that of mAb c13C6 (Pallesen et al., 2016), suggesting that these two mAbs share overlapping epitopes in the GP glycan cap (Figures 4D–E and S3–S4). Consistent with this hypothesis, binding of both ADI-15750 and c13C6 was sensitive to the G271R escape mutation engendered by ADI-15750 (Figure S4C–D).

The GP base-binding NAbs ADI-15878 and ADI-15742 are clonal siblings with 90% and 95% identity in their variable heavy (V_H) and variable light (V_L) amino acid sequences, respectively (Bornholdt et al., 2016) (Figure 6A). Their Fabs showed a steep angle of approach similar to the SUDV-monospecific Fab 16F6 (Dias, 2011), but appeared to be rotated by ≈90° about their long axes relative to the EBOV-monospecific Fab KZ52 (Figures 3B–C, I) (Lee et al., 2008b). The epitope targeted by ADI-15878 and ADI-15742 is also shifted by ≈60° about the central threefold axis of the GP trimer with respect to those of other well-characterized base binders, including KZ52, 16F6, c2G4 and c4G7 (Dias et al., 2011; Lee et al., 2008a; Murin et al., 2014; Pallesen et al., 2016) (Figures 3B–C, I and 4). The ADI-15878/15742 footprint on GP comprises discontinuous sequences in both GP1 and GP2 subunits that span neighboring protomers, including putative membrane-seeking residues in the highly conserved GP2 internal fusion loop (IFL) (Figures 3B–C and 4). Consistent with a critical role for NAb-IFL contacts, a single point mutation in the IFL, G528E, abolished both viral recognition and neutralization without observable effects on viral entry (Figures 3F–G and S2–S3). Interestingly, both ADI-15742 and ADI-15878 are also predicted to make extensive contacts with the complex N-liked glycan at GP2 residue 563, in the α–helical heptad repeat 1 (HR1) sequence of the adjacent protomer (Figures 3B, C, F, G and 4B). Glycosylation of this residue is strictly conserved across all known filovirus GP proteins (Figure S3), and its deletion is detrimental for assembly and viral incorporation of EBOV GP, suggesting that it is structurally important (Lennemann et al., 2015).

ADI-15946, the third broadly neutralizing base binder we identified, is directed toward an epitope that is similarly positioned to those of mAbs KZ52, c2G4 and c4G7 (Lee et al., 2008a; Murin et al., 2014; Pallesen et al., 2016), but shifted upwards towards the glycan cap (Figures 3D and 4F–H). Its angle of approach is similar to that of mAb c2G4 (Murin et al., 2014; Pallesen et al., 2016), and putative NAb contacts involve discontinuous sequences with a single GP protomer: GP1 base (residues 71–77), glycan cap (residues 251–303), and GP2 (residues 508-514) (Figures 3D and 4F). A single amino acid change (K510E), adjacent to the KZ52/c2G4/c4G7 escape mutation (Q508R) (Audet et al., 2014), afforded complete viral resistance to ADI-15946 binding

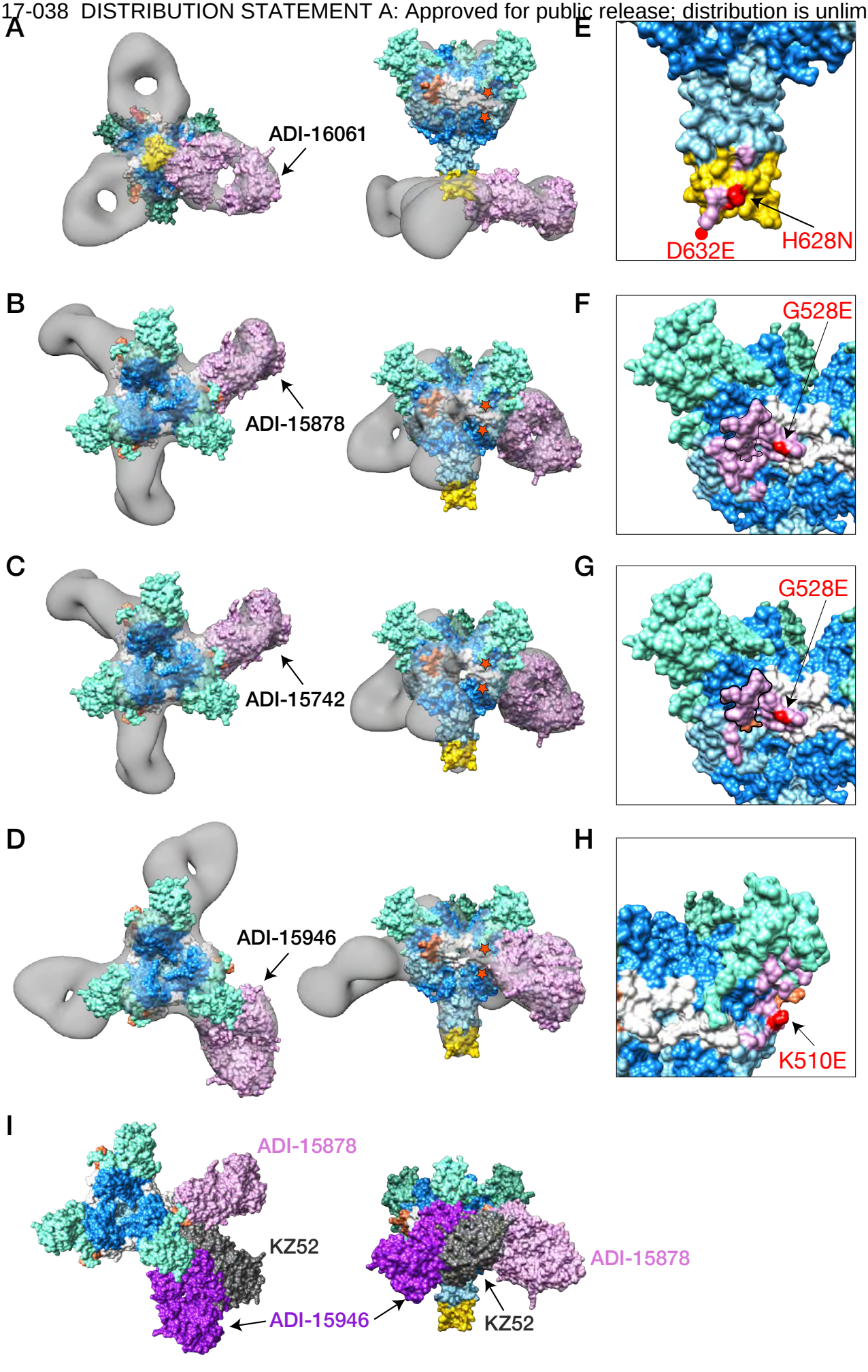
A
ADI-16061
E
D632E
H628N
B
ADI-15878
F
G528E
C
ADI-15742
G
G528E
D
ADI-15946
H
K510E
I
ADI-15878
KZ52
ADI-15946
ADI-15878
KZ52

Figure 3

Figure 3. Negative-stain electron microscopy of Fab: EBOV GPΔTM complexes

(A–D) 3D reconstructions of four Fab:EBOV GPΔTM complexes are shown in transparent surface representation (gray) with a structure-based model of the GPΔTM trimer [PDB: 5JQ3 (Zhao et al., 2016)] fitted into the density. Structural subdomains of the GP trimer have been mapped onto the structure as follows: GP1 glycan cap (aqua green), GP1 core (blue), GP2 (light blue), GP2 internal fusion loop region (white), and the stalk/HR2 region (yellow). The conserved glycan at GP2 residue Asn 563 is indicated in orange. Additionally, a structural model of each Fab variable region was generated using the ROSIE server (Lyskov et al., 2013; Sivasubramanian et al., 2009) and then fitted into the density map as a surface-shaded representation (lilac). The structure of each complex is shown as top (left) and side (right) views, with the exception of ADI-16061, which is shown from the bottom up, relative to the viral membrane. Orange stars in panels A–D indicate the approximate termini of the β13–14 loop that connects the GP1 base and glycan cap subdomains.

(E–H) Magnified views of panels A–D indicating the putative Fab contact sites on the GPΔTM trimer (lilac). Residues conferring viral neutralization escape are indicated in red. See also Figures S2–S3.

(I) 3D reconstructions of ADI-15878 and ADI-15946 are superimposed with a structure-based model of the GPΔTM:KZ52 Fab complex [PDB: 3CSY (Lee et al., 2008a)] to highlight the angle of approach of each base binder.

Figure 4

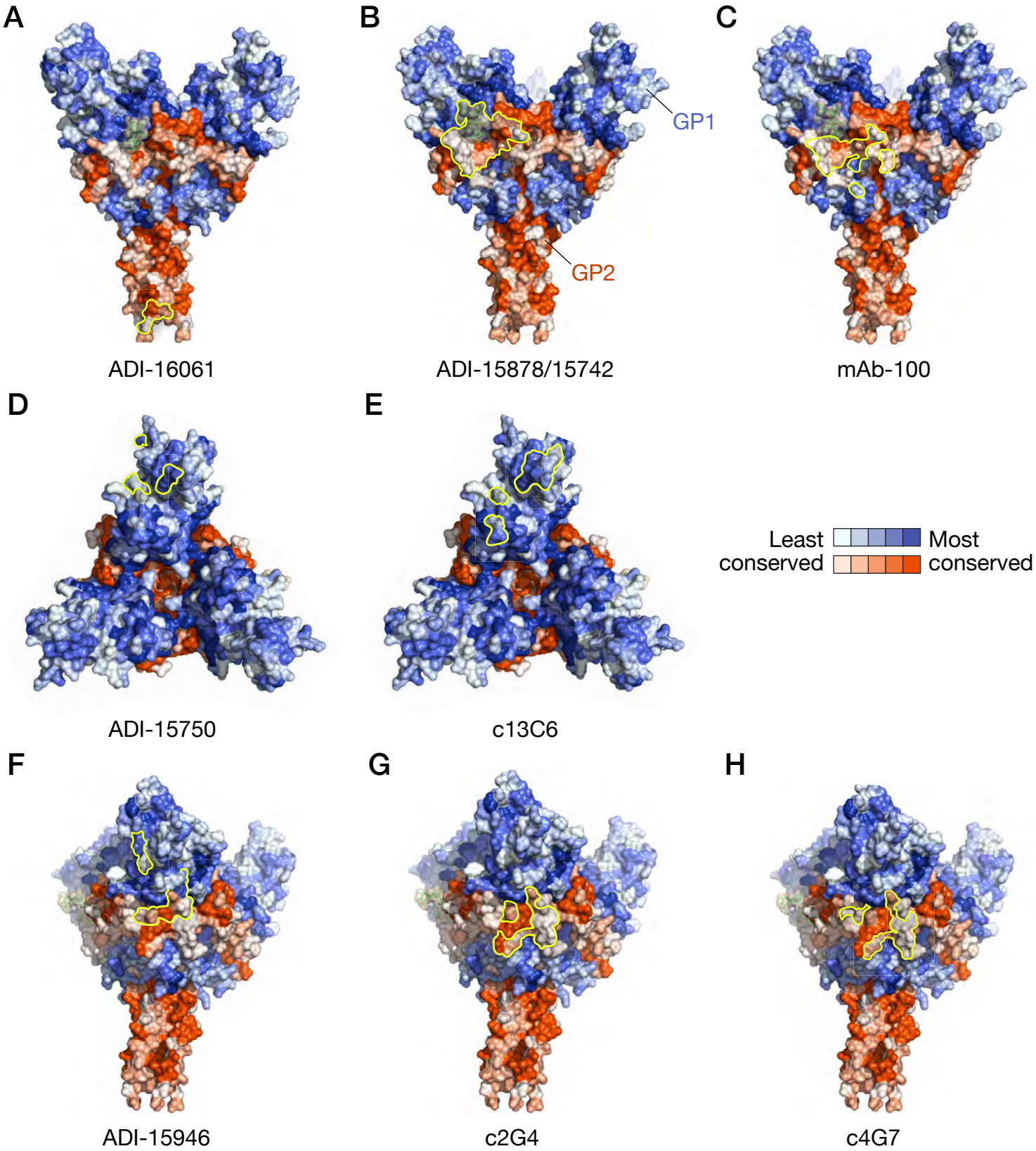
A
B
C
GP1
GP2
ADI-16061
ADI-15878/15742
mAb-100
D
E
Least conserved
Most conserved
ADI-15750
c13C6
F
G
H
ADI-15946
c2G4
c4G7

Figure 4. Predicted epitopes recognized by the broadly neutralizing human mAbs, and their sequence conservation among ebolaviruses

(A–H) The predicted GP contact surface for each NAb is indicated as a yellow outline on a surface-shaded representation of the GPΔTM trimer model (PDB: 5JQ3). Each amino acid residue in GP1 (blue) and GP2 (red) is shaded according to the degree of sequence conservation among filovirus GP proteins at that position, based on a multiple sequence alignment (light to dark, 0 to 100% sequence identity). In panels A–C, the N–linked glycan at GP2 residue Asn 563 is indicated as a translucent envelope and green balls-and-sticks. Antibody footprints in panels C, E, G, and H are derived from published structures of EBOV GP:Fab complexes (Lee et al., 2008a; Murin et al., 2014; Pallesen et al., 2016).

and neutralization (Figures 3D, H, S2–S3). A second mutation at a distinct, buried, position in the GP1 base (E100K) weakened viral neutralization by ADI-15946, but did not substantially diminish its capacity to bind to GP. The higher level of sequence conservation in the putative ADI-15946 epitope relative to those of c2G4, C4G7, and KZ52 likely explains the former's enhanced antiviral breadth (Figures 4F and S3D). However, the greater sequence divergence of SUDV and RESTV GP at the proposed sites of contact (Figure S3) is consistent with the failure of ADI-15946 to neutralize viruses bearing these GPs.

Mechanisms of antiviral neutralization

The filovirus cell entry pathway is a complex, multistep process that culminates in GP-catalyzed fusion between viral and host endosomal membranes, and escape of a viral nucleocapsid payload into the cytoplasm (Miller and Chandran, 2012; Moller-Tank and Maury, 2015). Following their attachment to the plasma membrane of a permissive host cell, filovirus virions are internalized into the endocytic system and trafficked to a late endo/lysosomal compartment (Mingo et al., 2015; Simmons et al., 2015; Spence et al., 2016). In endosomes, resident host cysteine cathepsins cleave GP to remove the mucin and glycan cap sequences (Chandran et al., 2005; Schornberg et al., 2006), thereby unmasking a binding site for the critical endosomal receptor, Niemann-Pick C1 (NPC1) (Bornholdt et al., 2015; Carette et al., 2011; Cote et al., 2011; Miller et al., 2012). Recognition of NPC1 by a cleaved GP species (hereafter, GP_{CL}), together with one or more unknown host signals, is proposed to trigger GP refolding and the membrane fusion reaction that is coupled to it (Brecher et al., 2012; Miller et al., 2012; Spence et al., 2016; Wong et al., 2010).

Because GP_{CL}-NPC1 recognition is a central, and indispensable, requirement for filovirus entry (Miller et al., 2012; Wang et al., 2016), we first examined the capacity of the GP base-binding NAbs to inhibit it in a competitive ELISA (Figure 5A). Pre-incubation of each NAb with VSV particles bearing EBOV GP_{CL} had no effect on viral capture of a soluble fragment of NPC1, whereas the mAbs MR72 and FVM04, which bind directly to sequences in the GP_{CL} receptor-binding site (RBS), blocked NPC1 capture, as described previously (Bornholdt et al., 2015; Howell et al., 2016). Thus, none of the GP base binders described in the current study exert their antiviral effect by directly preventing the virus-receptor interaction. This is consistent with the location of their epitopes at sites distant from the RBS, and with their apparent failure to induce large conformational changes upon GP binding (Figures 3–4).

Endosomal GP→GP_{CL} cleavage is a prerequisite for GP-NPC1 binding and therefore essential for filovirus entry. Accordingly, we next investigated if any of the NAbs could interfere with this proteolytic processing step, as reported for the human EBOV-specific GP base binders, KZ52 and mAb-100 (Misasi et al., 2016; Shedlock et al.,

2010). rVSV-EBOV GP particles were pre-incubated with each NAb and then exposed to the endosomal cysteine protease cathepsin L (CatL). GP cleavage was assessed by measuring exposure of the GP_{CL} RBS with an NPC1-binding ELISA (Figure 5B), or by gel electrophoresis and immunoblotting (Figure 5C), as described (Chandran et al., 2005; Miller et al., 2012). ADI-15946, similar to the ZMapp base binders c2G4 and c4G7, and to KZ52 and mAb-100, could inhibit GP→GP_{CL} cleavage and GP_{CL} RBS exposure in a dose-dependent manner. By contrast, ADI-15878 and ADI-15742 were ineffective at blocking the GP→GP_{CL} cleavage step. These results are consistent with the proximity of the binding footprints of mAb-100, c2G4, c4G7, and ADI-15946 to the GP1 β13–β14 loop, which is the initial target of proteolytic cleavage (Chandran et al., 2005; Dube et al., 2009; Lee et al., 2008a; Zhao et al., 2016). ADI-15878 and ADI-15742 do not appear to closely approach the β13–β14 loop (Figure 3B–D, I).

The preceding findings suggested that ADI-15878 and ADI-15742 act primarily at a step that follows GP→GP_{CL} cleavage and receptor engagement. Since an endosomally generated GP_{CL} species (either alone or in complex with NPC1) is the presumptive final target of these NAbs, we examined the capacities of the base binders to neutralize VSV particles bearing GP_{CL}, generated with CatL at pH 5.5 (Figure 5D). Strikingly, GP cleavage enhanced the antiviral potencies of ADI-15946, ADI-15878, and ADI-15742 by 50–200 fold (not shown for ADI-15742), whereas it attenuated or eliminated neutralization by the other base binders tested, KZ52, c2G4, and c4G7.

Kinetic binding studies by biolayer interferometry further elucidated pH- and cleavage-dependent changes in the GP binding affinity of some NAbs (Figure 5E). ADI-15878 bound with picomolar affinity to uncleaved GPΔTM at pH 7.5, but suffered a striking (10^3–10^4 fold) loss in binding affinity at pH 5.5, the presumptive pH of late endosomes. However, it regained picomolar binding affinity for CatL-cleaved GP_{CL}. ADI-15946 recognized uncleaved GPΔTM with nanomolar affinity at pH 7.5 and 5.5, and also gained picomolar binding to GP_{CL} at pH 5.5 (10^3–10^4-fold enhancement). Thus, the enhanced neutralization potential of these NAbs against cleaved viruses may be at least partially attributable to improvements in NAb:GP binding. Interestingly, however, the other base binders KZ52, c2G4, and c4G7, retained efficient binding to GP_{CL} despite their loss of neutralization potential against cleaved viruses, indicating that the nature of the epitope recognized, and not only binding affinity, dictates the molecular mechanism by which GP base-binding NAbs block ebolavirus entry.

Together, these results suggest that the broadly neutralizing base binders ADI-15878 and ADI-15742 differ from previously described monospecific base binders like KZ52, c2G4, and 4G7, in their ability to target and neutralize a cleaved GP species that is generated deep in the endocytic pathway (Figure 5F). Conversely, the latter base binders appear to act principally at and/or prior to the GP→GP_{CL} cleavage step. ADI-15946 displayed a dual behavior, and may act both upstream, to block GP cleavage,

Figure 5

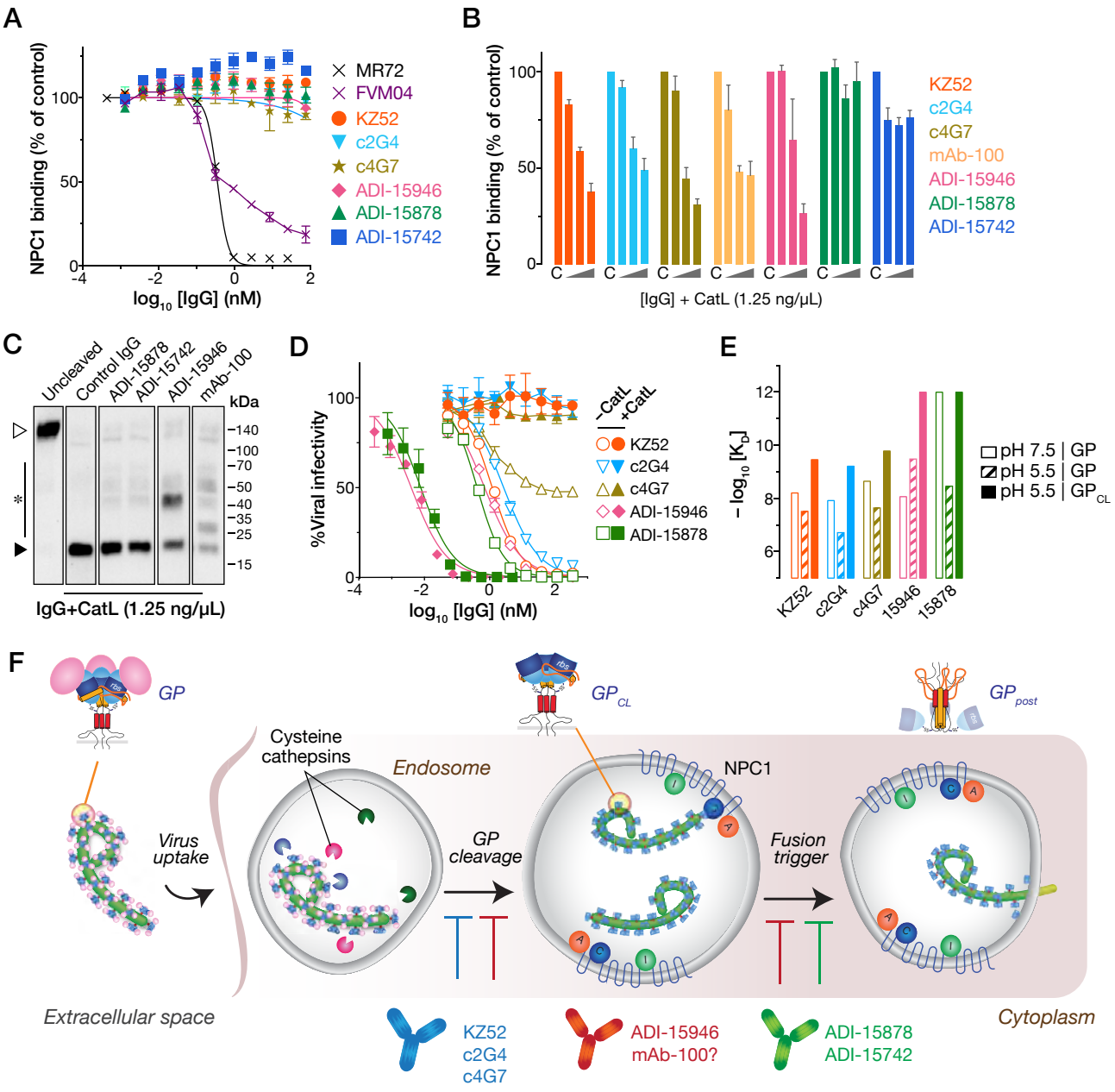
A
NPC1 binding (% of control)
log10 [IgG] (nM)
MR72
FVM04
KZ52
c2G4
c4G7
ADI-15946
ADI-15878
ADI-15742
B
NPC1 binding (% of control)
[IgG] + CatL (1.25 ng/μL)
KZ52
c2G4
c4G7
mAb-100
ADI-15946
ADI-15878
ADI-15742
C
Uncleaved
Control IgG
ADI-15878
ADI-15742
ADI-15946
mAb-100
kDa
IgG+CatL (1.25 ng/μL)
D
%Viral infectivity
log10 [IgG] (nM)
-CatL
+CatL
KZ52
c2G4
c4G7
ADI-15946
ADI-15878
E
– log10 [Kd]
pH 7.5 | GP
pH 5.5 | GP
pH 5.5 | GPCL
KZ52
c2G4
c4G7
15946
15878
F
GP
GPCL
GPpost
Cysteine cathepsins
Endosome
NPC1
Virus uptake
GP cleavage
Fusion trigger
Extracellular space
Cytoplasm
KZ52
c2G4
c4G7
ADI-15946
mAb-100?
ADI-15878
ADI-15742

Figure 5. Mechanistic basis of human mAb-dependent neutralization of ebolavirus entry

(A) Capacity of the NAbs to block EBOV GP_{CL}:NPC1 binding in an ELISA. Immobilized rVSV-EBOV GP_{CL} particles were incubated with increasing concentrations of each NAb and then with a pre-titrated concentration of purified NPC1 domain C-flag. Binding of NPC1 to GP_{CL} was detected with an anti-flag antibody. Means±SD for three replicates are shown.

(B) Capacity of the NAbs to block exposure of the NPC1-binding RBS mediated by GP→GP_{CL} cleavage. rVSV-EBOV GP particles were incubated with cathepsin L (CatL) at pH 5.5 in the presence of 50 nM, 250 nM, and 1000 nM NAb (total [IgG] was kept constant at 1000 nM by mixing with control human IgG1). GP:NPC1 binding was detected by NPC1 ELISA as in (A). Means±SD for six replicates from two pooled experiments are shown.

(C) Capacity of the NAbs to block EBOV GP→GP_{CL} cleavage. Reactions from (B) were resolved by SDS-PAGE and GP1 was visualized by western blotting. Open triangle, uncleaved GP1. Filled triangle, cleaved GP1. Asterisk, partially cleaved GP1 species.

(D) Capacity of NAbs to neutralize viruses bearing uncleaved or cleaved GP in a single-round infection assay. NAb neutralization dose curves of VSV-EBOV GP and CatL-generated VSV-EBOV GP_{CL} particles. Means±SD for three replicates are shown.

(E) Binding affinities of the NAbs for uncleaved and cleaved EBOV GPΔTM. Kinetic binding constants for NAb:GP and NAb:GP_{CL} binding were determined by biolayer interferometry. NAbs were loaded onto probes, which were then dipped in a solution containing serial dilutions of the GP or GP_{CL} analyte at the indicated pH values. See also Table S3 for kinetic binding constants.

(F) Schematic model for steps in ebolavirus entry targeted by the NAbs.

and downstream, to target one or more GP_{CL}-like species at or near the membrane fusion step (Figure 5F).

Germline origin of ADI-15878 and ADI-15742 and sequence determinants of their neutralization potency and breadth

ADI-15878 and ADI-15742 are the first known human mAbs with pan-ebolavirus neutralizing activity. To begin to define the molecular basis of their breadth of reactivity and neutralization, we assigned the V_H and V_L sequences of each NAb to their respective germline genes, and reverted ADI-15878 to its nearest inferred germline (IGL) precursor (Figure 6A). ADI-15878^{IGL} contained germline reversions in most framework and complementarity-determining regions (CDR) segments, but retained WT (fully mature) CDR-H3, because the originating germline sequence in this region could not be predicted with confidence given the highly diverse nature of D segments upon VDJ recombination. ADI-15878^{IGL} bound detectably to EBOV GPΔTM (K_D≈400 nM) by biolayer interferometry [BLI]), but it lacked neutralizing activity (Figures 6B–C, S5–S6). Heterodimeric light chain-heavy chain pairings containing one mature, somatic hypermutation (SHM)-bearing variable domain and one IGL variable domain bound to EBOV GP with single-digit nanomolar affinity (20–100 fold lower K_D), but picomolar affinity to EBOV GP required pairing of both mature chains (Figure S5B–D). The higher affinity of mature variable domains for binding to EBOV GP was primarily due to slower dissociation rates (k_{off}) relative to variants containing one or both IGL segments. These changes in binding affinity associated with SHM in the mature variable regions were accompanied by incremental improvements in neutralization potency and breadth. However, neutralization of viruses bearing SUDV and/or RESTV GP was more dependent on sequences containing SHMs, suggesting that ADI-15878 engages these divergent GPs with slightly different contacts (Figures 6C and S6). Together, these findings suggest that the CDRs of both V_H (non–CDR-H3) and V_L sequences of ADI-15878 and ADI-15742 make key contributions to both the energetics of ebolavirus GP binding, and to the pan-ebolavirus neutralizing efficacy of these NAbs.

To complement the above analysis, we separately assessed the contributions of individual CDR-H3 residues in ADI-15878 by alanine scanning mutagenesis (Figures 6B–C and S5–6). WT ADI-15878 mAb exhibited a slow off rate for both GP and GP_{CL} (accurate measurement could not be obtained by BLI, but was less than 10^{-7} s^{-1}), consistent with other high affinity antibodies, and providing a lower estimate of K_D of 1 pM against both forms of EBOV GP. Most of the WT→Ala CDR-H3 mutants exhibited dramatically lower binding to EBOV GP (K_Ds 20– to 74,000–fold higher than 1 pM), indicating that mutations were either detrimental to direct binding interactions or altered productive CDR-H3 loop conformations. However, all of the WT→Ala CDR-H3 mutants had only modest effects on neutralization potency against rVSV-EBOV GP relative to WT ADI-

Figure 6

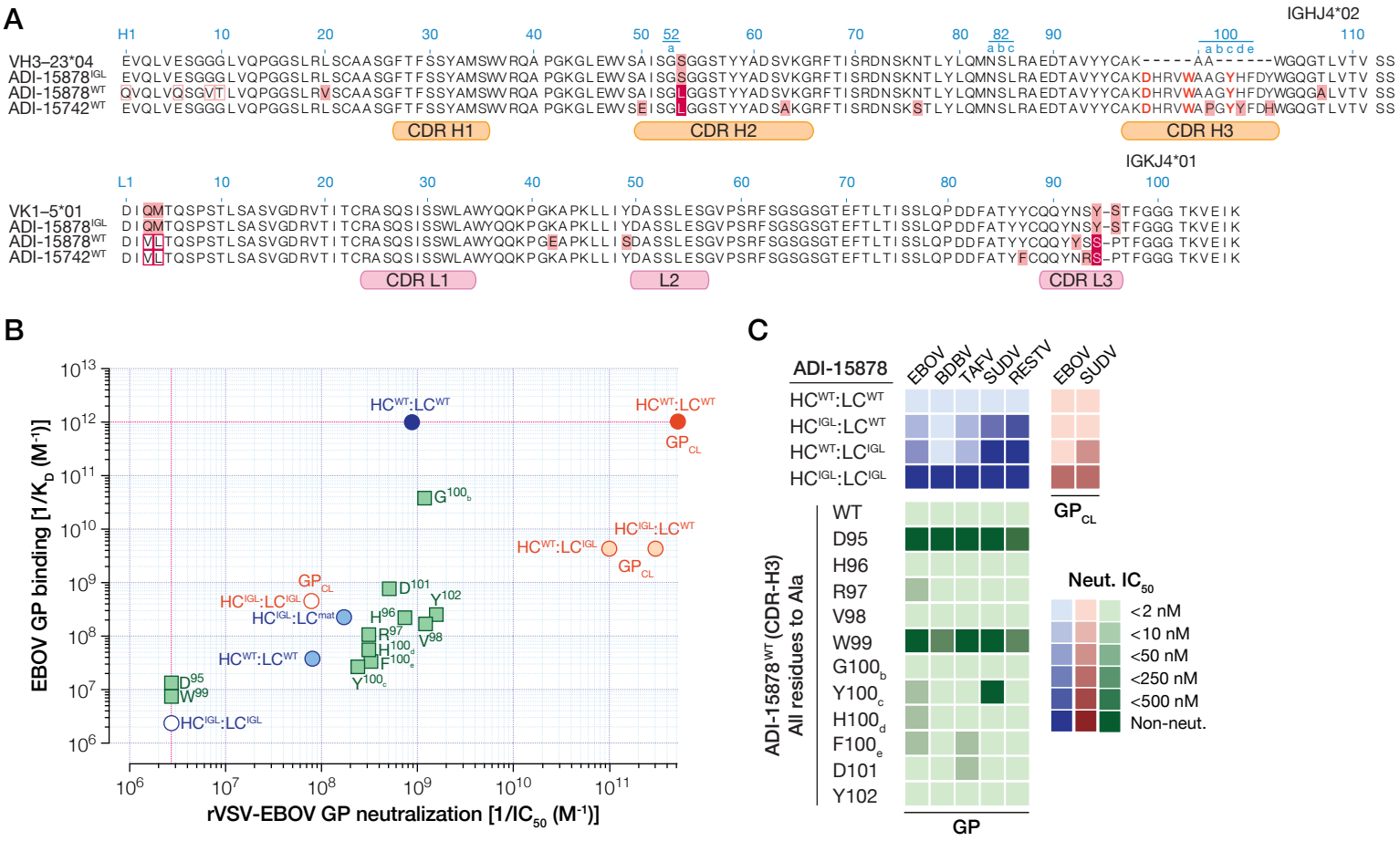
A
IGHJ4*02
VH3–23*04
ADI-15878IGL
ADI-15878WT
ADI-15742WT
CDR H1
CDR H2
CDR H3
IGKJ4*01
VK1–5*01
ADI-15878IGL
ADI-15878WT
ADI-15742WT
CDR L1
L2
CDR L3
B
EBOV GP binding [1/KD (M-1)]
rVSV-EBOV GP neutralization [1/IC50 (M-1)]
HCWT:LCWT
GPCL
HCIGL:LCWT
HCWT:LCIGL
HCIGL:LCIGL
HCIGL:LCmat
C
ADI-15878
EBOV
BDBV
TAFV
SUDV
RESTV
ADI-15878WT (CDR-H3)
All residues to Ala
WT
D95
H96
R97
V98
W99
D101
Y102
GP
Neut. IC50
<2 nM
<10 nM
<50 nM
<250 nM
<500 nM
Non-neut.

Figure 6. Germline origin of ADI-15878 and sequence determinants of its neutralizing activity

(A) Alignment of mature VH and VL sequences (ADI-15878^{mat}) with their closest human germline V and J gene segments, and reconstruction of an inferred germline ancestor (ADI-15878^{IGL}) bearing mature CDR-H3. Amino acid residues at positions divergent from the inferred germline sequence are shaded in pink, and changes shared by both WT ADI-15878 and ADI-15742 are shaded in maroon. Residues in open boxes indicate primer-induced mutations. Residues in CDR-H3 critical for viral neutralization are highlighted in red. Light and heavy chain sequences are numbered according to the Kabat scheme.

(B) Comparison of the equilibrium dissociation constant (K_D) for NAb binding to GP and GP_{CL}, to each NAb's capacity to neutralize rVSV-EBOV GP infection (IC_{50}). Blue and orange circles, ADI-15878^{WT}, ADI-15878^{IGL}, and their HC:LC chimeras vs. EBOV GP and GP_{CL}, respectively. Green squares, ADI-15878 bearing mutations in CDR-H3. Pink lines indicate high and low limits of detection for binding K_D and neutralization IC_{50}, respectively. Also see panel C and Figures S5–S6.

(C) Heat maps for neutralization of rVSVs bearing ebolavirus GP and GP_{CL} proteins by the indicated ADI-15878 variants. Also see panel B and Figure S6.

15878, except D95A and W99A, which suffered a ≈99% reduction in potency. These neutralization trends extended to GPs from the other ebolaviruses, except for $Y100_cA$, which was selectively less potent against rVSV-SUDV GP (Figure S5C–D). These results suggest that interactions between the CDR-H3 loop of ADI-15878 and structurally conserved elements in GP2 IFL and HR1 contribute to pan-ebolavirus recognition and neutralization. Furthermore, they identify three WT side chains (D95, W99, $Y100_c$) that are critical to the pan-ebolavirus neutralizing activity of ADI-15878.

Protective efficacy in animal models of EBOV, SUDV, and BDBV challenge

We assessed the protective efficacy of the broadly neutralizing human NAbs in three small-animal models of lethal ebolavirus challenge (Figure 7). First, wild type (WT) BALB/c mice were exposed to mouse-adapted EBOV (EBOV-MA), and then administered a single dose of each NAb at 2 days post-infection (300 μg/animal; ≈15 mg/kg) (Figure 7A–B). Cross-neutralizing NAbs from each epitope group were highly (≥80%) protective against EBOV in this stringent post-exposure setting, with little or no weight loss apparent in NAb-treated animals.

We next evaluated the NAbs in the Type I interferon α/β receptor-deficient mouse model for SUDV challenge (Figure 7C–D) (Brannan et al., 2015). Mice were exposed to WT SUDV, and then dosed with each NAb on days 1 and 4 post-infection (300 μg/animal/dose; ≈15 mg/kg). The pan-ebolavirus NAbs ADI-15878 and ADI-15742 afforded ≥95% survival and greatly reduced weight loss, relative to the PBS control group. By contrast, the HR2 binder ADI-16061 and the base binder ADI-15946, both weak SUDV neutralizers, provided little or no protection against SUDV. To the contrary, ADI-16061 significantly increased mortality in two independent experiments ($p<0.05$), raising the possibility that it can enhance SUDV infection *in vivo*.

Finally, we tested the anti-BDBV efficacy of the two pan-ebolavirus human NAbs, ADI-15878 and ADI-15742, in the domestic ferret, which is the only described non-NHP model for BDBV challenge (Figure 7E–F) (Cross et al., 2016; Kozak et al., 2016). Animals received two doses of each NAb (15 mg and 10 mg per animal on days 3 and 6 post-challenge, respectively). As observed previously (Cross et al., 2016; Kozak et al., 2016), BDBV infection was uniformly lethal, with PBS-treated animals succumbing between days 8–10 following challenge. By contrast, both NAbs afforded highly significant levels of survival ($p<0.01$; 3 of 4 animals for ADI-15878; 2 of 4 for ADI-15742). Furthermore, peak viremia levels correlated with NAb treatment and survival outcome, with lower viral titers observed in the surviving animals relative to those that succumbed to infection ($p<0.001$), and in NAb-treated animals relative to PBS-treated controls ($p<0.001$). Viremia also trended lower in animals receiving ADI-15878 relative to those receiving ADI-15742, but this difference did not reach statistical significance. In sum, our findings demonstrate that the pan-ebolavirus NAbs ADI-15878 and ADI-

Figure 7

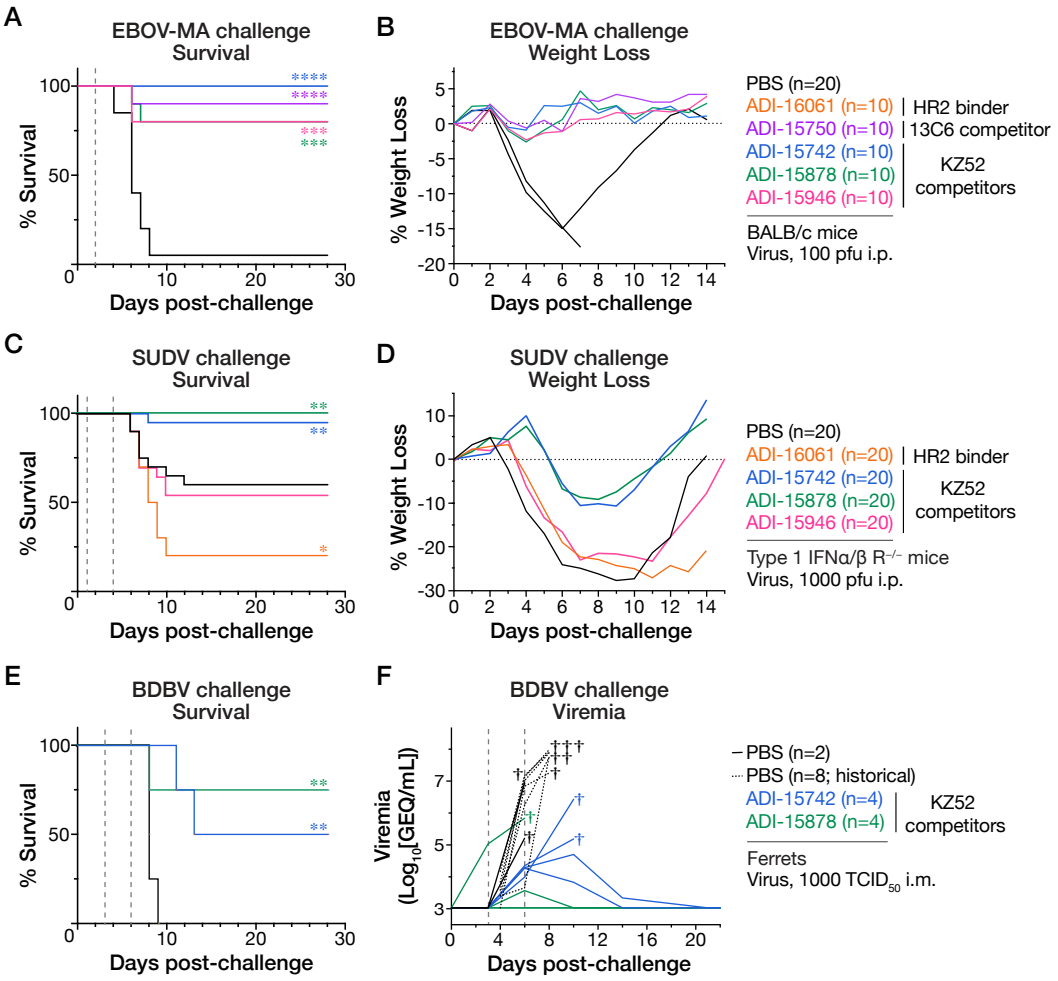
A
EBOV-MA challenge
Survival
% Survival
Days post-challenge
B
EBOV-MA challenge
Weight Loss
% Weight Loss
Days post-challenge
PBS (n=20)
ADI-16061 (n=10)
ADI-15750 (n=10)
ADI-15742 (n=10)
ADI-15878 (n=10)
ADI-15946 (n=10)
HR2 binder
13C6 competitor
KZ52 competitors
BALB/c mice
Virus, 100 pfu i.p.
C
SUDV challenge
Survival
% Survival
Days post-challenge
D
SUDV challenge
Weight Loss
% Weight Loss
Days post-challenge
PBS (n=20)
ADI-16061 (n=20)
ADI-15742 (n=20)
ADI-15878 (n=20)
ADI-15946 (n=20)
HR2 binder
KZ52 competitors
Type 1 IFNα/β R−/− mice
Virus, 1000 pfu i.p.
E
BDBV challenge
Survival
% Survival
Days post-challenge
F
BDBV challenge
Viremia
Viremia (Log10[GEQ/mL])
Days post-challenge
PBS (n=2)
PBS (n=8; historical)
ADI-15742 (n=4)
ADI-15878 (n=4)
KZ52 competitors
Ferrets
Virus, 1000 TCID50 i.m.

Figure 7. *In vivo* protective efficacy of broadly neutralizing human mAbs

(A) BALB/c mice were challenged with mouse-adapted EBOV (EBOV-MA), and then treated with a single dose of each NAb (300 μg; ≈15 mg/kg) or vehicle (PBS) at 2 days post-challenge.

(B) Weight loss curves for control and NAb-treated groups in panel A.

(C) Type 1 IFNα /β $R^{-/-}$ mice were challenged with WT SUDV, and then treated with two doses of each NAb (300 μg per dose, ≈15 mg/kg) or vehicle (PBS) at 1 and 4 days post-challenge.

(D) Weight loss curves for control and NAb-treated groups in panel C.

(E) Ferrets were challenged with WT BDBV, and then treated with two doses of each NAb (15 mg and 10 mg, respectively) or vehicle (PBS) at 3 and 6 days post-challenge.

(F) Longitudinal measurements of plasma viremia in infected ferrets from panel E (GEQ, viral genome equivalents). Cross symbol indicates deceased animal.

In panels A, C, and E, 'n' indicates the number of animals per group. Survival in each group was compared to that in the PBS vehicle group by log-rank (Mantel-Cox) test (*, $p<0.05$; **, $p<0.01$; ***, $p<0.001$; ****, $p<0.0001$). All other comparisons to the PBS group were not significant.

15742 can afford post-exposure protection against challenge by the three divergent ebolaviruses currently associated with lethal disease outbreaks in humans.

DISCUSSION

Herein, we investigated the antiviral breadth of the neutralizing antibody response in a human survivor of the 2013–2016 West African EBOV epidemic. Although predominantly restricted to EBOV GP (i.e., monospecific), this response contained a small proportion of mAbs (<10%) that could neutralize GPs derived from three or more ebolaviruses, as also observed for a mAb panel isolated from a survivor of BDBV infection (Flyak et al., 2016). Whereas the cross-neutralizers reported by Flyak and co-workers (2016) were largely found to recognize the apical glycan cap subdomain of GP, we uncovered cross-neutralizing mAbs that also targeted other structural regions of the trimeric GP spike, namely the base, comprising closely apposed sequences in GP1 and GP2, and the stalk, comprising the second heptad repeat sequence (HR2) and the viral membrane-proximal extracellular region (MPER) of GP2. The broadest and most potent of the NAbs identified in our screen recognized base epitopes. ADI-15878 and ADI-15742, two clonally-related mAbs of the 349 screened, afforded highly potent neutralizing activity (IC_{50}<1 nM) against all five known ebolaviruses, including the three associated with disease outbreaks in humans (EBOV, BDBV, and SUDV). A third base binder, ADI-15946, could neutralize four of five ebolaviruses (all except RESTV), but demonstrated only modest potency against SUDV.

ADI-15878 and ADI-15742 recognize a novel epitope in the GP base that comprises hydrophobic membrane-seeking residues at the “tip” of the GP2 internal fusion loop (IFL), as well as more C–terminal residues in the first heptad repeat (HR1) sequence of the neighboring GP2 subunit. Unusually, both mAbs also appear to contact a highly conserved and functionally critical N–linked glycan at residue N563 in HR1. The recognition of a more conserved GP2 surface, and in particular, a reduced dependence on the highly variable sequences at the GP2 N–terminus, probably explains the increased antiviral breadth of ADI-15878/ADI-15742 relative to the prototypic base binders KZ52, c2G4, and c4G7 (Figure 4 and S3). Interestingly, the recently described human mAb-100 binds to the same face of the GP trimer as ADI-15878/ADI-15742 (rotated 60˚ about GP’s threefold axis of symmetry with respect to KZ52, c2G4, and c4G7) (Misasi et al., 2016). However, mAb-100 contacts residues—including some in the IFL—that vary more extensively among ebolaviruses (Figure 4C), which may account for its limited neutralization breadth (Misasi et al., 2016) (M.J. Aman, personal communication). Serial viral passage in the presence of ADI-15878 elicited the escape mutation G528E in the IFL, which was also observed in selections with the broadly neutralizing mouse mAb 6D6 (Furuyama et al., 2016), suggesting that, although the GP:6D6 complex has

not yet been structurally elucidated, ADI-15878 and 6D6 share similar epitopes. Together, these two antibodies point to a shared solution for pan-ebolavirus neutralization that targets a critical and highly conserved element of the GP membrane fusion machinery.

Our findings further define the antiviral mechanisms of GP base-binding NAbs, and point to novel modes of neutralization by ADI-15878, ADI-15742, and ADI-15946 (Figure 5F). In contrast to the base binders KZ52, c2G4, c4G7, and mAb-100, ADI-15878/15742 did not inhibit GP→GP_{CL} cleavage, likely reflecting the latter's lack of proximity to the initial sites of cleavage in the GP1 β13–β14 loop (Figure 3F). Instead, these NAbs displayed dramatically enhanced neutralization of viral particles containing GP_{CL} in concert with increased binding affinity for GP_{CL}, whereas KZ52, c2G4, and c4G7 lost most or all of their antiviral potency. These results are consistent with a model in which both the prototypic base binders and ADI-15878/15742 recognize GP with high affinity at neutral pH and are delivered to endosomes together with viral particles. Here, however, their mechanisms of action diverge. The prototypic base binders may act only at one or more upstream steps in entry, as also proposed by Misasi and colleagues (2016), whereas ADI-15878 and ADI-15742 appear to principally target a cleaved GP intermediate (Figure 5F). The latter mAbs do not block the GP_{CL}:NPC1 interaction. Rather, their protomer-spanning mode of binding is predicted to "lock" the cleaved GP trimer, whether free or bound to NPC1, in a pre-fusion state, thereby arresting GP conformational changes required for viral membrane fusion.

ADI-15946, which recognizes a GP surface proximal to the epitopes of KZ52, c2G4, and c4G7, shares features with both these prototypic base binders and ADI-15878/15742. ADI-15946 resembled KZ52, c2G4, and c4G7 in inhibiting GP→GP_{CL} cleavage, but unlike them, and like ADI-15878/15742, it displayed heightened neutralization potency against cleaved viruses. We speculate that, by binding GP1 residues adjacent to the RBS (71–77) (Figures 4F and S3D) that were shown to rearrange upon GP_{CL}:NPC1 association (Wang et al., 2016), ADI-15946 may arrest the transduction of receptor-induced conformational changes required for fusion triggering. KZ52, c2G4, and c4G7 do not appear to make such GP1 contacts (Figure 4G, H) (Bornholdt et al., 2015; Murin et al., 2014; Pallesen et al., 2016).

Here we report the first human mAbs with potent pan-ebolavirus neutralizing activity. Prior to this work, the only such canonical mAb known (6D6) was of non-human origin, and it was elicited through a complex immunization scheme with heterologous viral antigens (Furuyama et al., 2016). To explore the genesis of such mAbs in humans infected with a single ebolavirus, we characterized "germline-reverted" variants of ADI-15878 for viral binding and neutralization. Our results suggest that, although ADI-15878/15742-like pan-ebolavirus neutralizing mAbs did not arise with high frequency in this human survivor of Ebola virus disease (2/349), the barrier for maturation of such

mAbs may be lower than that seen in some other viral diseases. ADI-15878 and ADI-15742 originate from the most common germline heavy chain segment (VH3-23), do not possess extremely long CDR-H3s (15 amino acids vs. 20–33 for broadly neutralizing HIV-1–specific mAbs whose epitopes contain protein sequences and glycans), and require only a few SHMs for broad and potent antiviral activity (≈6% amino acid changes in V_H vs. ≈30% for HIV-1 CD4-binding site—specific NAbs) (Bornholdt et al., 2016; Corti and Lanzavecchia, 2013; Tiller et al., 2013). Furthermore, a germline-reverted variant of ADI-15878 (albeit with a mature CDR-H3) could recognize EBOV GP with submicromolar affinity (Figures 6 and S5). Finally, because this human survivor was presumably only exposed to a single filovirus, EBOV/Makona, our findings and those of others (Flyak et al., 2016) imply that the diversity of NAbs within a typical polyclonal primary response to ebolavirus infection is large enough to contain at least some with broad and potent activity. This contrasts with broadly neutralizing mAbs against HIV-1, which originate in human subjects who control long-term infection (presumably via the action of such mAbs), or those against dengue virus, which were isolated from patients with active secondary infections (Corti and Lanzavecchia, 2013; Dejnirattisai et al., 2015). Thus, our results may warrant future larger-scale explorations of the antiviral breadth of circulating filovirus-specific antibody repertoires in humans. They also raise the possibility that some survivors of Ebola virus disease harbor aspects of memory immunity that could confer broad protection against other members of this viral family.

Our findings further suggest the possibility of eliciting broadly neutralizing anti-ebolavirus mAbs efficiently in humans through immunization with a suitably engineered immunogen, since the sites of broad vulnerability within GP are clearly defined, and the generation of ADI-15878/15742-like responses requires only subtle maturation of an abundantly represented germline. Interestingly, the germline-reverted ADI-15878 variant could bind with single-digit nanomolar K_D to soluble EBOV GP_{CL} (Figures 6C and S5A). Its increased binding affinity for GP_{CL} over GP was driven by a ≈100-fold increase in association rate constant (Figure S5C), likely resulting from removal of the steric bulk of the glycan cap and mucin domain sequences. Remarkably, this variant retained broad neutralizing activity against viruses bearing GP_{CL} (Figure 6C and S6A). We thus hypothesize that minimized EBOV GP constructs that mimic GP_{CL} in some respects may preferentially elicit ADI-15878/15742-like antibodies, both through enhanced activation of the appropriate B-cell precursors and by removal of putatively immunodominant sequences in the glycan cap and mucin domain. Such engineered germline-targeting immunogens may have utility as part of a broadly protective next-generation vaccine against filoviruses.

ADI-15878 and ADI-15742 are the first mAbs shown to protect against EBOV, BDBV, and SUDV in animal models of ebolavirus challenge under stringent post-exposure conditions when administered as monotherapy, and our results suggest that

they should also afford protection against other ebolaviruses. To mitigate the risk associated with the generation of viral neutralization escape variants, we propose that cocktails comprising ADI-15878 or ADI-15742 and at least one other pan-protective, but non-competing, human mAb would provide ideal candidates for the development of a broadly effective therapy to prevent and treat ebolavirus infections. Finally, we speculate that cocktails combining pan–GP-specific NAbs that arrest filovirus entry at distinct upstream and downstream steps (Figure 5F) may act synergistically to confer especially potent antiviral protection.

AUTHOR CONTRIBUTIONS

A.Z.W., A.S.H., C.D.M., E.K.N., D.M.A., J.M.F., S.H., R.M.J., M.A.D.L.V., R.R.B., E.G., H.L.T., L.Z., R.K.J., X.Q., J.R.L., L.M.W., A.B.W., J.M.D., K.C., and Z.A.B. designed research, analyzed data, and wrote and/or edited the paper. E.G. and L.M.W. designed the germline-reverted constructs and E.G., L.M.W., A.Z.W., D.M.A., and Z.M.B. produced GPs and mAbs for structural and functional studies. A.Z.W., E.K.N., J.M.F., R.K.J., D.M.A., and Z.A.B. characterized the binding, neutralization, and other functional properties of the mAbs. C.D.M., H.L.T., and A.B.W. performed structural studies on GP:Fab complexes. A.S.H., R.M.J., and R.R.B. performed the mouse challenge studies. S.H., M.A.D.L.V., and X.Q. performed the ferret challenge studies.

ACKNOWLEDGMENTS

We thank C. Harold, T. Alkutkar, and T.B. Krause for technical assistance. We thank M.J. Aman for his comments on the manuscript and for his kind gift of mAb h21D10. Support for this work was provided by NIH grants U19 AI109762 (Centers for Excellence in Translational Research) to K.C., J.R.L., J.M.D., A.B.W., and L.Z., DTRA contract HDTRA1-13-C-0018 to L.Z., D.M.A., and Z.A.B., and DTRA contract CB4077 to A.S.H., R.R.B., R.M.J. and J.M.D. This work was also supported by Public Health Agency of Canada. E.K.N. was also supported by a DAAD (Deutscher Akademischer Austauschdienst, German Academic Exchange Service) fellowship. Opinions, conclusions, interpretations, and recommendations are those of the authors and are not necessarily endorsed by the U.S. Army. The mention of trade names or commercial products does not constitute endorsement or recommendation for use by the Department of the Army or the Department of Defense.

REFERENCES

Audet, J., Wong, G., Wang, H., Lu, G., Gao, G.F., Kobinger, G., and Qiu, X. (2014). Molecular characterization of the monoclonal antibodies composing ZMAb: a protective cocktail against Ebola virus. Sci Rep *4*, 6881.

Bornholdt, Z.A., Ndungo, E., Fusco, M.L., Bale, S., Flyak, A.I., Crowe, J.E., Jr., Chandran, K., and Saphire, E.O. (2015). Host-Primed Ebola Virus GP Exposes a Hydrophobic NPC1 Receptor-Binding Pocket, Revealing a Target for Broadly Neutralizing Antibodies. MBio *7*.

Bornholdt, Z.A., Turner, H.L., Murin, C.D., Li, W., Sok, D., Souders, C.A., Piper, A.E., Goff, A., Shamblin, J.D., Wollen, S.E.*, et al.* (2016). Isolation of potent neutralizing antibodies from a survivor of the 2014 Ebola virus outbreak. Science *351*, 1078-1083.

Brannan, J.M., Froude, J.W., Prugar, L.I., Bakken, R.R., Zak, S.E., Daye, S.P., Wilhelmsen, C.E., and Dye, J.M. (2015). Interferon alpha/beta Receptor-Deficient Mice as a Model for Ebola Virus Disease. J Infect Dis.

Bray, M., Davis, K., Geisbert, T., Schmaljohn, C., and Huggins, J. (1998). A mouse model for evaluation of prophylaxis and therapy of Ebola hemorrhagic fever. J Infect Dis *178*, 651-661.

Brecher, M., Schornberg, K.L., Delos, S.E., Fusco, M.L., Saphire, E.O., and White, J.M. (2012). Cathepsin cleavage potentiates the Ebola virus glycoprotein to undergo a subsequent fusion-relevant conformational change. J Virol *86*, 364-372.

Burk, R., Bollinger, L., Johnson, J.C., Wada, J., Radoshitzky, S.R., Palacios, G., Bavari, S., Jahrling, P.B., and Kuhn, J.H. (2016). Neglected filoviruses. FEMS Microbiol Rev *40*, 494-519.

Carette, J.E., Raaben, M., Wong, A.C., Herbert, A.S., Obernosterer, G., Mulherkar, N., Kuehne, A.I., Kranzusch, P.J., Griffin, A.M., Ruthel, G.*, et al.* (2011). Ebola virus entry requires the cholesterol transporter Niemann-Pick C1. Nature *477*, 340-343.

Chandran, K., Sullivan, N.J., Felbor, U., Whelan, S.P., and Cunningham, J.M. (2005). Endosomal proteolysis of the Ebola virus glycoprotein is necessary for infection. Science *308*, 1643-1645.

Corti, D., and Lanzavecchia, A. (2013). Broadly neutralizing antiviral antibodies. Annu Rev Immunol *31*, 705-742.

Cote, M., Misasi, J., Ren, T., Bruchez, A., Lee, K., Filone, C.M., Hensley, L., Li, Q., Ory, D., Chandran, K.*, et al.* (2011). Small molecule inhibitors reveal Niemann-Pick C1 is essential for Ebola virus infection. Nature *477*, 344-348.

Cross, R.W., Mire, C.E., Borisevich, V., Geisbert, J.B., Fenton, K.A., and Geisbert, T.W. (2016). The Domestic Ferret (Mustela putorius furo) as a Lethal Infection Model for 3 Species of Ebolavirus. J Infect Dis *214*, 565-569.

de La Vega, M.A., Stein, D., and Kobinger, G.P. (2015). Ebolavirus Evolution: Past and Present. PLoS Pathog *11*, e1005221.

Dejnirattisai, W., Wongwiwat, W., Supasa, S., Zhang, X., Dai, X., Rouvinski, A., Jumnainsong, A., Edwards, C., Quyen, N.T., Duangchinda, T.*, et al.* (2015). A new class of highly potent, broadly neutralizing antibodies isolated from viremic patients infected with dengue virus. Nat Immunol *16*, 170-177.

Dias, J.M., Kuehne, A.I., Abelson, D.M., Bale, S., Wong, A.C., Halfmann, P., Muhammad, M.A., Fusco, M.L., Zak, S.E., Kang, E.*, et al.* (2011). A shared structural solution for neutralizing ebolaviruses. Nat Struct Mol Biol *18*, 1424-1427.

Dube, D., Brecher, M.B., Delos, S.E., Rose, S.C., Park, E.W., Schornberg, K.L., Kuhn, J.H., and White, J.M. (2009). The primed ebolavirus glycoprotein (19-kilodalton GP1,2): sequence and residues critical for host cell binding. J Virol *83*, 2883-2891.

Flyak, A.I., Shen, X., Murin, C.D., Turner, H.L., David, J.A., Fusco, M.L., Lampley, R., Kose, N., Ilinykh, P.A., Kuzmina, N.*, et al.* (2016). Cross-Reactive and Potent Neutralizing Antibody Responses in Human Survivors of Natural Ebolavirus Infection. Cell *164*, 392-405.

Frei, J.C., Nyakatura, E.K., Zak, S.E., Bakken, R.R., Chandran, K., Dye, J.M., and Lai, J.R. (2016). Bispecific Antibody Affords Complete Post-Exposure Protection of Mice from Both Ebola (Zaire) and Sudan Viruses. Sci Rep *6*, 19193.

Furuyama, W., Marzi, A., Nanbo, A., Haddock, E., Maruyama, J., Miyamoto, H., Igarashi, M., Yoshida, R., Noyori, O., Feldmann, H.*, et al.* (2016). Discovery of an antibody for pan-ebolavirus therapy. Sci Rep *6*, 20514.

Goddard, T.D., Huang, C.C., and Ferrin, T.E. (2007). Visualizing density maps with UCSF Chimera. J Struct Biol *157*, 281-287.

Group, P.I.W., and Multi-National, P.I.I.S.T. (2016). A Randomized, Controlled Trial of ZMapp for Ebola Virus Infection. N Engl J Med *375*, 1448-1456.

Howell, K.A., Qiu, X., Brannan, J.M., Bryan, C., Davidson, E., Holtsberg, F.W., Wec, A.Z., Shulenin, S., Biggins, J.E., Douglas, R.*, et al.* (2016). Antibody Treatment of Ebola and Sudan Virus Infection via a Uniquely Exposed Epitope within the Glycoprotein Receptor-Binding Site. Cell Rep.

Jahrling, P.B., Geisbert, T.W., Geisbert, J.B., Swearengen, J.R., Bray, M., Jaax, N.K., Huggins, J.W., LeDuc, J.W., and Peters, C.J. (1999). Evaluation of immune globulin and recombinant interferon-alpha2b for treatment of experimental Ebola virus infections. J Infect Dis *179 Suppl 1*, S224-234.

Keck, Z.Y., Enterlein, S.G., Howell, K.A., Vu, H., Shulenin, S., Warfield, K.L., Froude, J.W., Araghi, N., Douglas, R., Biggins, J.*, et al.* (2015). Macaque Monoclonal Antibodies Targeting Novel Conserved Epitopes within Filovirus Glycoprotein. J Virol *90*, 279-291.
Kozak, R., He, S., Kroeker, A., de La Vega, M.A., Audet, J., Wong, G., Urfano, C., Antonation, K., Embury-Hyatt, C., Kobinger, G.P.*, et al.* (2016). Ferrets Infected with Bundibugyo Virus or Ebola Virus Recapitulate Important Aspects of Human Filovirus Disease. J Virol *90*, 9209-9223.
Kuhn, J.H., Andersen, K.G., Baize, S., Bao, Y., Bavari, S., Berthet, N., Blinkova, O., Brister, J.R., Clawson, A.N., Fair, J.*, et al.* (2014). Nomenclature- and database-compatible names for the two Ebola virus variants that emerged in Guinea and the Democratic Republic of the Congo in 2014. Viruses *6*, 4760-4799.
Lander, G.C., Stagg, S.M., Voss, N.R., Cheng, A., Fellmann, D., Pulokas, J., Yoshioka, C., Irving, C., Mulder, A., Lau, P.W.*, et al.* (2009). Appion: an integrated, database-driven pipeline to facilitate EM image processing. J Struct Biol *166*, 95-102.
Lee, J.E., Fusco, M.L., Hessell, A.J., Oswald, W.B., Burton, D.R., and Saphire, E.O. (2008a). Structure of the Ebola virus glycoprotein bound to an antibody from a human survivor. Nature *454*, 177-182.
Lee, J.E., Kuehne, A., Abelson, D.M., Fusco, M.L., Hart, M.K., and Saphire, E.O. (2008b). Complex of a protective antibody with its Ebola virus GP peptide epitope: unusual features of a V lambda x light chain. J Mol Biol *375*, 202-216.
Lennemann, N.J., Walkner, M., Berkebile, A.R., Patel, N., and Maury, W. (2015). The Role of Conserved N-Linked Glycans on Ebola Virus Glycoprotein 2. J Infect Dis.
Lyskov, S., Chou, F.C., Conchuir, S.O., Der, B.S., Drew, K., Kuroda, D., Xu, J., Weitzner, B.D., Renfrew, P.D., Sripakdeevong, P.*, et al.* (2013). Serverification of molecular modeling applications: the Rosetta Online Server that Includes Everyone (ROSIE). PLoS One *8*, e63906.
Macneil, A., Reed, Z., and Rollin, P.E. (2011). Serologic cross-reactivity of human IgM and IgG antibodies to five species of Ebola virus. PLoS Negl Trop Dis *5*, e1175.
Miller, E.H., and Chandran, K. (2012). Filovirus entry into cells - new insights. Curr Opin Virol *2*, 206-214.
Miller, E.H., Obernosterer, G., Raaben, M., Herbert, A.S., Deffieu, M.S., Krishnan, A., Ndungo, E., Sandesara, R.G., Carette, J.E., Kuehne, A.I.*, et al.* (2012). Ebola virus entry requires the host-programmed recognition of an intracellular receptor. EMBO J *31*, 1947-1960.
Mingo, R.M., Simmons, J.A., Shoemaker, C.J., Nelson, E.A., Schornberg, K.L., D'Souza, R.S., Casanova, J.E., and White, J.M. (2015). Ebola virus and severe acute respiratory syndrome coronavirus display late cell entry kinetics: evidence that transport to NPC1+ endolysosomes is a rate-defining step. J Virol *89*, 2931-2943.
Misasi, J., Gilman, M.S., Kanekiyo, M., Gui, M., Cagigi, A., Mulangu, S., Corti, D., Ledgerwood, J.E., Lanzavecchia, A., Cunningham, J.*, et al.* (2016). Structural and molecular basis for Ebola virus neutralization by protective human antibodies. Science *351*, 1343-1346.
Moller-Tank, S., and Maury, W. (2015). Ebola virus entry: a curious and complex series of events. PLoS Pathog *11*, e1004731.
Murin, C.D., Fusco, M.L., Bornholdt, Z.A., Qiu, X., Olinger, G.G., Zeitlin, L., Kobinger, G.P., Ward, A.B., and Saphire, E.O. (2014). Structures of protective antibodies reveal sites of vulnerability on Ebola virus. Proc Natl Acad Sci U S A *111*, 17182-17187.
Natesan, M., Jensen, S.M., Keasey, S.L., Kamata, T., Kuehne, A.I., Stonier, S.W., Lutwama, J.J., Lobel, L., Dye, J.M., and Ulrich, R.G. (2016). Human Survivors of Disease Outbreaks Caused by Ebola or Marburg Virus Exhibit Cross-Reactive and Long-Lived Antibody Responses. Clin Vaccine Immunol *23*, 717-724.
Ng, M., Ndungo, E., Jangra, R.K., Cai, Y., Postnikova, E., Radoshitzky, S.R., Dye, J.M., Ramirez de Arellano, E., Negredo, A., Palacios, G.*, et al.* (2014). Cell entry by a novel European filovirus requires host endosomal cysteine proteases and Niemann-Pick C1. Virology *468-470*, 637-646.
Ogura, T., Iwasaki, K., and Sato, C. (2003). Topology representing network enables highly accurate classification of protein images taken by cryo electron-microscope without masking. J Struct Biol *143*, 185-200.
Ou, W., Delisle, J., Jacques, J., Shih, J., Price, G., Kuhn, J.H., Wang, V., Verthelyi, D., Kaplan, G., and Wilson, C.A. (2012). Induction of ebolavirus cross-species immunity using retrovirus-like particles bearing the Ebola virus glycoprotein lacking the mucin-like domain. Virol J *9*, 32.
Pallesen, J., Murin, C.D., de Val, N., Cottrell, C.A., Hastie, K.M., Turner, H.L., Fusco, M.L., Flyak, A.I., Zeitlin, L., Crowe, J.E., Jr.*, et al.* (2016). Structures of Ebola virus GP and sGP in complex with therapeutic antibodies. Nat Microbiol *1*, 16128.
Qiu, X., Wong, G., Audet, J., Bello, A., Fernando, L., Alimonti, J.B., Fausther-Bovendo, H., Wei, H., Aviles, J., Hiatt, E.*, et al.* (2014). Reversion of advanced Ebola virus disease in nonhuman primates with ZMapp. Nature *514*, 47-53.
Regula, L.K., Harris, R., Wang, F., Higgins, C.D., Koellhoffer, J.F., Zhao, Y., Chandran, K., Gao, J., Girvin, M.E., and Lai, J.R. (2013). Conformational properties of peptides corresponding to the ebolavirus GP2 membrane-proximal external region in the presence of micelle-forming surfactants and lipids. Biochemistry *52*, 3393-3404.
Schornberg, K., Matsuyama, S., Kabsch, K., Delos, S., Bouton, A., and White, J. (2006). Role of endosomal cathepsins in entry mediated by the Ebola virus glycoprotein. J Virol *80*, 4174-4178.

Shedlock, D.J., Bailey, M.A., Popernack, P.M., Cunningham, J.M., Burton, D.R., and Sullivan, N.J. (2010). Antibody-mediated neutralization of Ebola virus can occur by two distinct mechanisms. Virology *401*, 228-235.
Simmons, J.A., D'Souza, R.S., Ruas, M., Galione, A., Casanova, J.E., and White, J.M. (2015). Ebolavirus Glycoprotein Directs Fusion through NPC1+ Endolysosomes. J Virol *90*, 605-610.
Sivasubramanian, A., Sircar, A., Chaudhury, S., and Gray, J.J. (2009). Toward high-resolution homology modeling of antibody Fv regions and application to antibody-antigen docking. Proteins *74*, 497-514.
Spence, J.S., Krause, T.B., Mittler, E., Jangra, R.K., and Chandran, K. (2016). Direct Visualization of Ebola Virus Fusion Triggering in the Endocytic Pathway. MBio *7*.
Suloway, C., Pulokas, J., Fellmann, D., Cheng, A., Guerra, F., Quispe, J., Stagg, S., Potter, C.S., and Carragher, B. (2005). Automated molecular microscopy: the new Leginon system. J Struct Biol *151*, 41-60.
Takada, A., Robison, C., Goto, H., Sanchez, A., Murti, K.G., Whitt, M.A., and Kawaoka, Y. (1997). A system for functional analysis of Ebola virus glycoprotein. Proc Natl Acad Sci U S A *94*, 14764-14769.
Tang, G., Peng, L., Baldwin, P.R., Mann, D.S., Jiang, W., Rees, I., and Ludtke, S.J. (2007). EMAN2: an extensible image processing suite for electron microscopy. J Struct Biol *157*, 38-46.
Tiller, T., Schuster, I., Deppe, D., Siegers, K., Strohner, R., Herrmann, T., Berenguer, M., Poujol, D., Stehle, J., Stark, Y*., et al.* (2013). A fully synthetic human Fab antibody library based on fixed VH/VL framework pairings with favorable biophysical properties. MAbs *5*, 445-470.
Towner, J.S., Sealy, T.K., Khristova, M.L., Albarino, C.G., Conlan, S., Reeder, S.A., Quan, P.L., Lipkin, W.I., Downing, R., Tappero, J.W*., et al.* (2008). Newly discovered ebola virus associated with hemorrhagic fever outbreak in Uganda. PLoS Pathog *4*, e1000212.
Voss, N.R., Yoshioka, C.K., Radermacher, M., Potter, C.S., and Carragher, B. (2009). DoG Picker and TiltPicker: software tools to facilitate particle selection in single particle electron microscopy. J Struct Biol *166*, 205-213.
Wang, H., Shi, Y., Song, J., Qi, J., Lu, G., Yan, J., and Gao, G.F. (2016). Ebola Viral Glycoprotein Bound to Its Endosomal Receptor Niemann-Pick C1. Cell *164*, 258-268.
Wec, A.Z., Nyakatura, E.K., Herbert, A.S., Howell, K.A., Holtsberg, F.W., Bakken, R.R., Mittler, E., Christin, J.R., Shulenin, S., Jangra, R.K*., et al.* (2016). A "Trojan horse" bispecific antibody strategy for broad protection against ebolaviruses. Science.
Wong, A.C., Sandesara, R.G., Mulherkar, N., Whelan, S.P., and Chandran, K. (2010). A forward genetic strategy reveals destabilizing mutations in the Ebolavirus glycoprotein that alter its protease dependence during cell entry. J Virol *84*, 163-175.
Wong, G., and Kobinger, G.P. (2015). Backs against the wall: novel and existing strategies used during the 2014-2015 Ebola virus outbreak. Clin Microbiol Rev *28*, 593-601.
Zhao, Y., Ren, J., Harlos, K., Jones, D.M., Zeltina, A., Bowden, T.A., Padilla-Parra, S., Fry, E.E., and Stuart, D.I. (2016). Toremifene interacts with and destabilizes the Ebola virus glycoprotein. Nature *535*, 169-172.

MATERIALS AND METHODS

Cells

Vero African grivet monkey cells and 293T human embryonic kidney fibroblast cells were maintained in high-glucose Dulbecco's modified Eagle medium (DMEM; Thermo Fisher) supplemented with 10% fetal bovine serum (Atlanta Biologicals), 1% GlutaMAX (Thermo Fisher), and 1% penicillin-streptomycin (Thermo Fisher). Cells were maintained in a humidified 37°C, 5% CO2 incubator.

Vesicular stomatitis virus (VSV) recombinants and pseudotypes

Recombinant vesicular stomatitis Indiana viruses (rVSV) expressing eGFP in the first position, and encoding representative GP proteins from EBOV/Mayinga (EBOV/H.sap-tc/COD/76/Yambuku-Mayinga), EBOV/Makona (EBOV/H.sap-rec/LBR/14/Makona-L2014), BDBV (BDBV/H.sap/UGA/07/But-811250), SUDV/Boneface (SUDV/C.por-lab/SSD/76/Boneface), RESTV (RESTV/M.fas-tc/USA/89/Phi89-AZ-1435), and LLOV (LLOV/M.sch-wt/ESP/03/Asturias-Bat86), in place of VSV G have been described previously (Ng et al., 2014; Wec et al., 2016; Wong et al., 2010). VSV pseudotypes bearing eGFP and GP proteins from TAFV (TAFV/H.sap-tc/CIV/94/CDC807212) and MARV (MARV/H.sap-tc/KEN/80/Mt. Elgon-Musoke) were generated as described (Takada et al., 1997).

Generation of cleaved VSV-GP particles and GPΔTM ectodomain proteins

In some experiments, cleaved viral particles bearing GP_{CL} were first generated by incubation with thermolysin (200 µg/mL, pH 7.5, 37˚C for 1 h; Sigma-Aldrich) or recombinant human cathepsin L (CatL, 2 ng/µL, pH 5.5, 37˚C for 1 h; R&D Systems), as described previously (Wong et al., 2010). Reactions were stopped by removal onto ice and addition of phosphoramidon (1 mM) or E-64 (10 µM), respectively, and viral particles were used immediately for infectivity assays. A recombinant, soluble GPΔTM protein (Bornholdt et al., 2016) was also essentially as described above.

VSV infectivity measurements and neutralization assays

Viral infectivities were measured by automated counting of eGFP+ cells (infectious units; IU) using a CellInsight CX5 imager (Thermo Fisher) at 12–14 h post-infection. For mAb neutralization experiments, pre-titrated amounts of VSV-GP particles (MOI ≈1 IU per cell) were incubated with increasing concentrations of test mAb at room temp for 1 h, and then added to confluent cell monolayers in 96-well plates. Viral neutralization data were subjected to nonlinear regression analysis to derive EC_{50} values (4-parameter, variable slope sigmoidal dose-response equation; GraphPad Prism).

Authentic filoviruses and microneutralization assays

The authentic filoviruses EBOV/"Zaire 1995" (EBOV/H.sap-tc/COD/95/Kik-9510621) (Jahrling et al., 1999), mouse-adapted EBOV/Mayinga (EBOV-MA) (Bray et al., 1998), SUDV/Boneface-USAMRIID111808, and BDBV/200706291 (Towner et al., 2008) were used in this study. Antibodies were diluted to indicated concentrations in culture media and incubated with virus for 1 h. Vero E6 cells were exposed to antibody/virus inoculum at an MOI of 0.2 (EBOV, BDBV) or 0.5 (SUDV) plaque-forming unit (PFU)/cell for 1 h. Antibody/virus inoculum was then removed and fresh culture media was added. At 48 h post-infection, cells were fixed, and infected cells were immunostained and quantitated by automated fluorescence microscopy, as described (Wec et al., 2016).

Generation of mAbs

Recombinant mAbs from the human EBOV disease survivor, as well as germline-reverted (IGL) mAb constructs and WT:IGL chimeras of ADI-15878 were expressed in *Saccharomyces cerevisiae* and purified from cell supernatants by protein A affinity chromatography, as described previously (Bornholdt et al., 2016). Other recombinant mAbs were produced in 293F cells by transient transfection, and purified by protein A affinity chromatography, as described previously (Wec et al., 2016).

ELISAs for GP:mAb binding

To identify GP cross-reactive mAbs in Figures 1 and S1, normalized amounts of rVSVs bearing EBOV, BDBV, and SUDV GP were coated onto plates at 4˚C. Plates were then blocked with PBS containing 3% bovine serum albumin (PBSA), and incubated with dilutions of test antibody (5, 50 nM). Bound Abs were detected with anti-human IgG conjugated to horseradish peroxidase (Santa Cruz Biotechnology) and Ultra-TMB colorimetric substrate (Thermo Fisher). All incubations were performed for 1 h at 37˚C.

Competition ELISAs for GP/mAb binding to NPC1

The viral lipid envelopes of rVSV-EBOV GP particles were labeled with biotin using a function-spacer-lipid construct (FSL-biotin) (Sigma-Aldrich) for 1 h at pH 7.5 and 37˚C, as described (Ng et al., 2014). Biotinylated viral particles bearing GP_{CL} were generated by incubation with thermolysin, and then captured onto high-binding 96-well ELISA plates precoated with recombinant streptavidin (0.65 µg/mL; Sigma-Aldrich). Plates were then blocked with PBSA, and incubated with serial dilutions of test mAbs. Washed plates were then incubated with a pre-titrated concentration of soluble, FLAG epitope-tagged, NPC1 domain C (NPC1–C) protein (Bornholdt et al., 2015), and bound NPC1–C was detected with an anti-FLAG antibody conjugated to horseradish peroxidase (Sigma-Aldrich). All incubations were performed for 1 h at 37˚C.

ELISAs and immunoblots to detect mAb inhibition of GP cleavage

In Figure 5B, we used exposure of the NPC1-binding site in EBOV GP_{CL} as a proxy for successful GP→GP_{CL} cleavage by CatL. rVSV-EBOV GP particles, biotinylated as above, were preincubated with mixtures of test mAb and irrelevant human IgG (test mAb at 50, 250, or 1000 nM; 1000 nM total IgG per reaction) for 1 h at pH 5.5 and 37°C. Reactions were then incubated with CatL (4 ng/µL and 37°C for 30 min). Reactions were then stopped with E-64, readjusted to neutral pH with PBS, and captured onto streptavidin-coated ELISA plates. NPC1–C binding was measured as above.

Samples treated with the highest concentration of test mAb were also subjected to western blotting (Figure 5C). Cleaved GP1 species were detected by immunoblotting with h21D10 mAb (a gift from Dr. Javad Aman) directly conjugated to horseradish peroxidase.

Selection of viral neutralization escape mutants

Escape mutant selections were performed by serial passage of rVSV-GP particles in the presence of test mAb. Briefly, serial 3-fold dilutions of virus were preincubated with a concentration of mAb corresponding to the IC_{90} value derived from neutralization assays, and then added to confluent monolayers of Vero cells in 12-well plates, in duplicate. Infection was allowed to proceed to completion (>90% cell death by eye), and supernatants were harvested from the infected wells that received the highest dilution (i.e., the least amount) of viral inoculum. Following three subsequent passages under mAb selection with virus-containing supernatants as above, supernatants from passage 4 were tested for viral neutralization escape. If resistance was evident, individual viral clones were plaque-purified on Vero cells, and their *GP* gene sequences were determined as described previously (Wong et al., 2010). The following escape mutant selections were performed: ADI-16061 with rVSV-EBOV/Makona GP, ADI-15742 with rVSV-SUDV/Boneface GP, ADI-15750 with rVSV-EBOV/Mayinga GP, and ADI-15946 with mucin domain-deleted rVSV-BDBV GPΔMuc.

Single-particle electron microscopy

Antibody Fabs and a EBOV GPΔTM ectodomain protein were prepared as described previously (Bornholdt et al., 2016), and incubated at a ratio of 10:1 (Fab:GP) overnight at 4°C. Complexes were then deposited onto a carbon-coated copper mesh grid, and stained with 1% uranyl formate. Samples were imaged on a Tecnai F12 microscope using the automated image acquisition software Leginon (Suloway et al., 2005). Images were collected with a Tietz 4K CMOS detector at 52,000× magnification, resulting in a final pixel size of 2.05Å at the specimen level. Images were automatically uploaded to and processed within our Appion database (Lander et al., 2009). Individual complexes were extracted from raw images using DoG Picker (Voss et al., 2009), binned by 2, and placed into a stack. The stack was then subjected to reference-free 2D classification

using MRA/MSA (Ogura et al., 2003). Class averages that did not respond to Fab:EBOV GPΔTM complexes were removed from all subsequent analyses. A subset of 2D class averages was used to create an initial model using common lines within EMAN2 (Tang et al., 2007). The raw particle stack was then refined against the initial model using EMAN2 to yield the final 3D volumes. UCSF Chimera was used for modeling and figure generation (Goddard et al., 2007).

GP:mAb kinetic binding analysis by biolayer interferometry (BLI)

The OctetRed™ system (ForteBio, Pall LLC) was used to determine the binding properties of different IgGs to various forms of EBOV GP. Anti-human Fc (AHC) capture sensors (ForteBio) were used for initial mAb loading at 25 mg/mL in 1× kinetics buffer (PBS supplemented with 0.002% Tween-20 and 1 mg/mL of BSA). Binding to GP was performed across two-fold serial dilutions of EBOV GPΔTM or GP_{CL}. The baseline and dissociation steps were carried out in the 1× kinetics buffer as per the instrument manufacturer's recommendations. For analysis of binding at pH 5.5, a 1× pH 5.5 kinetics buffer (50 mM sodium citrate dihydrate[pH 5.5], 150 mM sodium chloride, 0.002% Tween-20 and 1 mg/mL BSA) was used in place of the PBS-based 1× kinetic buffer for all steps. For all of the kinetics experiments, a global data fitting to a 1:1 binding model was used to estimate values for the k_{on} (association rate constant), k_{off} (dissociation rate constant), and K_D (equilibrium dissociation constant).

EBOV and SUDV challenge studies in mice

10–12 week old female BALB/c mice (Jackson Labs) were challenged via the intraperitoneal (i.p.) route with EBOV-MA (100 PFU; ~3,000 LD_{50}). Mice were treated i.p. 2 days post-challenge with PBS vehicle or 300 µg of each mAb (0.3 mL volume, ≈15 mg mAb/kg). Animals were observed daily for clinical signs of disease and lethality. Daily observations were increased to a minimum of twice daily while mice were exhibiting signs of disease. Moribund mice were humanely euthanized on the basis of IACUC-approved criteria.

6–8 week old male and female Type 1 IFN α/β receptor knockout mice (Type 1 IFNα/β R–/–) (Jackson Labs) were challenged with WT SUDV (1000 PFU i.p.). Animals were treated i.p. 1 and 4 days post-challenge with PBS vehicle or 300 µg (≈15 mg mAb/kg) per dose, and monitored and euthanized as above.

BDBV challenge studies in ferrets

Six-month-old female ferrets (*Mustela putorius furo*) were challenged via the intramuscular (i.m.) route with WT BDBV (BDBV/H.sap-tc/UGA/07/Butalya-811250; 1000 $TCID_{50}$ in 0.5 mL volume), as described previously (Kozak et al., 2016). Animals were treated i.p. 3 and 6 days post-challenge with either PBS vehicle or 15 mg (day 3) and 10 mg

(day 6) of each mAb (2 mL volume/dose). Additionally, 1 mL blood was taken from each animal on days 0, 3, 6, 10, 14, 21, 28 days post-infection to determine viral load, measure complete blood counts, and evaluate biochemical markers. Animals were monitored twice daily for signs of disease during the course of the experiment.

Animal welfare statement

Murine challenge studies were conducted under IACUC-approved protocols in compliance with the Animal Welfare Act, PHS Policy, and other applicable federal statutes and regulations relating to animals and experiments involving animals. The facility where these studies was conducted (USAMRIID) is accredited by the Association for Assessment and Accreditation of Laboratory Animal Care, International (AAALAC) and adhere to principles stated in the Guide for the Care and Use of Laboratory Animals, National Research Council, 2011.

Ferret challenge studies were approved by the Animal Care Committee (ACC) of the Canadian Science Centre for Human and Animal Health (CSCHAH) in Winnipeg, Canada, in accordance with guidelines from the Canadian Council on Animal Care (CCAC).

Statistical analysis

Dose-response neutralization curves were fit to a logistic equation by nonlinear regression analysis. 95% confidence intervals (95% CI) for the extracted IC_{50} parameter were estimated under the assumption of normality. Analysis of survival curves in Figure 7 was performed with the Mantel-Cox (log-rank) test. Statistical comparisons of viral titers in Figure 7F were carried out with an unpaired t-test. Testing level (alpha) was 0.05 for all statistical tests. All analyses were carried out in GraphPad Prism.

Figure S1

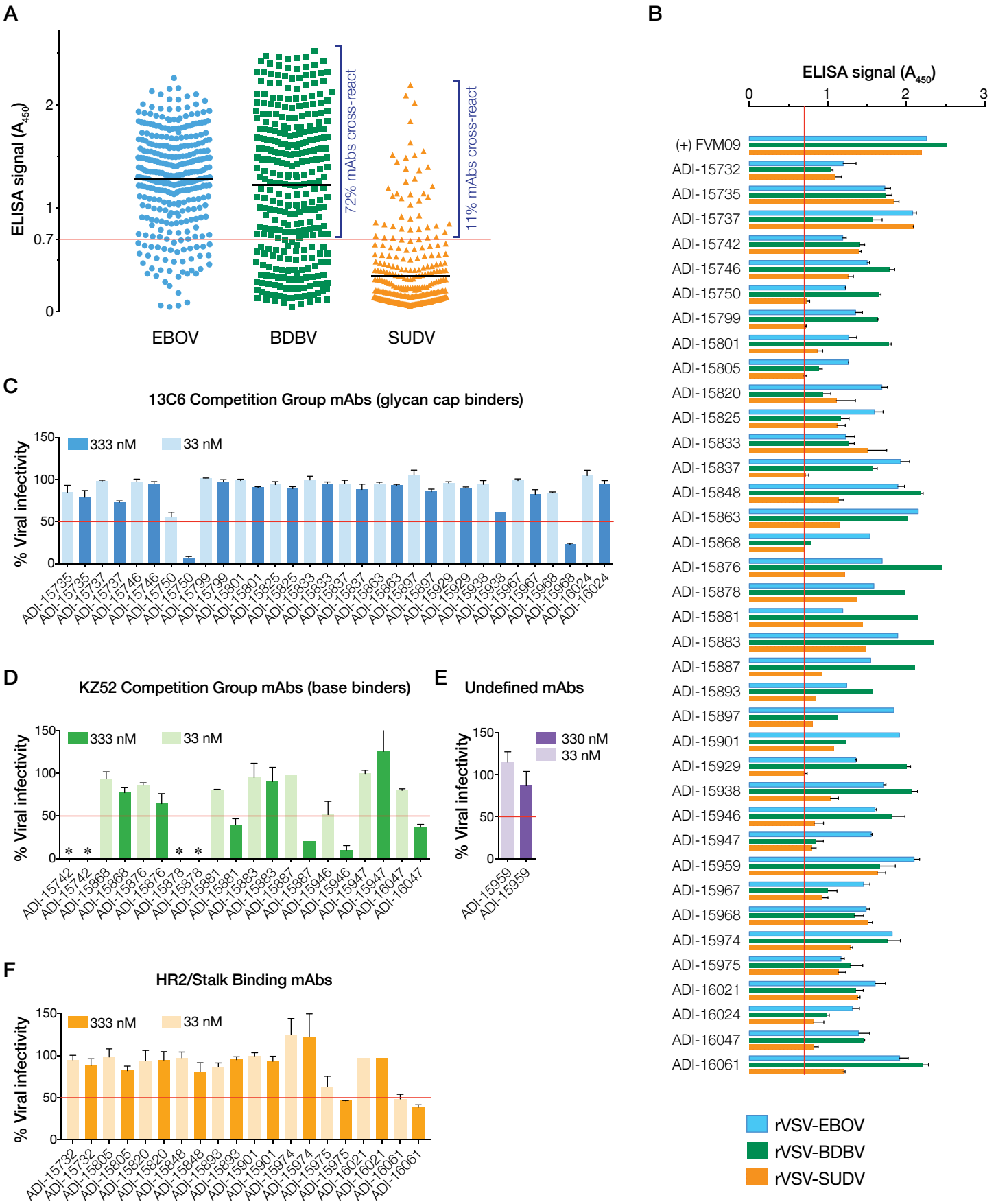
A
ELISA signal (A450)
72% mAbs cross-react
11% mAbs cross-react
EBOV
BDBV
SUDV
B
ELISA signal (A450)
(+) FVM09
ADI-15732
ADI-15735
ADI-15737
ADI-15742
ADI-15746
ADI-15750
ADI-15799
ADI-15801
ADI-15805
ADI-15820
ADI-15825
ADI-15833
ADI-15837
ADI-15848
ADI-15863
ADI-15868
ADI-15876
ADI-15878
ADI-15881
ADI-15883
ADI-15887
ADI-15893
ADI-15897
ADI-15901
ADI-15929
ADI-15938
ADI-15946
ADI-15947
ADI-15959
ADI-15967
ADI-15968
ADI-15974
ADI-15975
ADI-16021
ADI-16024
ADI-16047
ADI-16061
rVSV-EBOV
rVSV-BDBV
rVSV-SUDV
C
13C6 Competition Group mAbs (glycan cap binders)
% Viral infectivity
333 nM
33 nM
D
KZ52 Competition Group mAbs (base binders)
% Viral infectivity
333 nM
33 nM
E
Undefined mAbs
% Viral infectivity
330 nM
33 nM
F
HR2/Stalk Binding mAbs
% Viral infectivity
333 nM
33 nM

Figure S1. Screening a collection of 349 human EBOV survivor mAbs for pan-ebolavirus binders and neutralizers, related to Figure 1

(A) Capacity of mAbs to recognize rVSVs bearing EBOV, BDBV, and SUDV GP in an ELISA. A_{450}, absorbance at 450 nm. Red line indicates ELISA reactivity threshold for selecting cross-reactive mAbs, equivalent to 33% of the positive control.

(B) mAbs cross-reactive with SUDV GP in panel A were assayed for binding to rVSVs bearing EBOV, BDBV, and SUDV GP by ELISA. Means±SD for three replicates are shown. Red line indicates ELISA reactivity threshold for selecting cross-reactive mAbs.

(C–F) Capacity of cross-reactive mAbs to neutralize rVSV-SUDV GP infection at two mAb concentrations. Means ± standard deviation (SD) for three replicates are shown. Asterisks, infectivity below the detection limit. Red line indicates neutralization efficacy threshold for selecting cross-neutralizing mAbs. mAbs are binned by competition/epitope group.

Figure S2

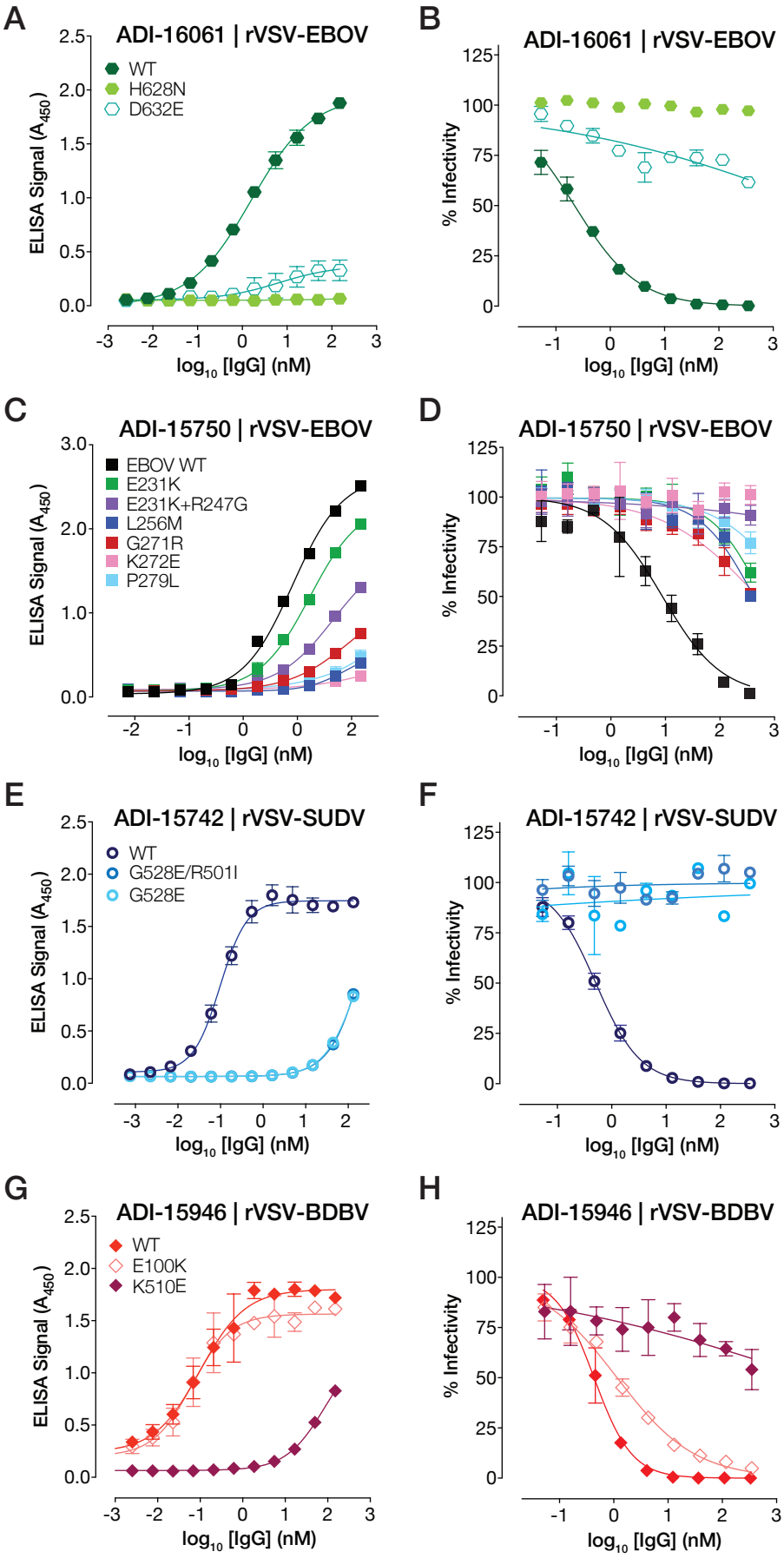
A
ADI-16061 | rVSV-EBOV
WT
H628N
D632E
ELISA Signal (A450)
log10 [IgG] (nM)
B
ADI-16061 | rVSV-EBOV
% Infectivity
log10 [IgG] (nM)
C
ADI-15750 | rVSV-EBOV
EBOV WT
E231K
E231K+R247G
L256M
G271R
K272E
P279L
ELISA Signal (A450)
log10 [IgG] (nM)
D
ADI-15750 | rVSV-EBOV
% Infectivity
log10 [IgG] (nM)
E
ADI-15742 | rVSV-SUDV
WT
G528E/R501I
G528E
ELISA Signal (A450)
log10 [IgG] (nM)
F
ADI-15742 | rVSV-SUDV
% Infectivity
log10 [IgG] (nM)
G
ADI-15946 | rVSV-BDBV
WT
E100K
K510E
ELISA Signal (A450)
log10 [IgG] (nM)
H
ADI-15946 | rVSV-BDBV
% Infectivity
log10 [IgG] (nM)

Figure S2. Characterization of viral mutants resistant to mAb neutralization, related to Figure 3

rVSV-GP mutants resistant to each broadly neutralizing mAb were selected and isolated as described in Materials and Methods.

(A, C, E, G) Capacity of NAbs to recognize rVSVs bearing GP neutralization-escape variants in an ELISA. Means±SD for three replicates are shown.

(B, D, F, H) Capacity of NAbs to neutralize rVSVs bearing GP neutralization-escape variants. Means±SD for three replicates are shown.

Figure S3

A

ADI-16061 putative epitope + escape mutants (original residue→mutant residue)

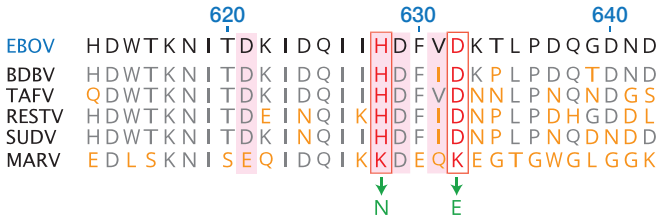

B

ADI-15750 escape mutants (original residue→mutant residue)

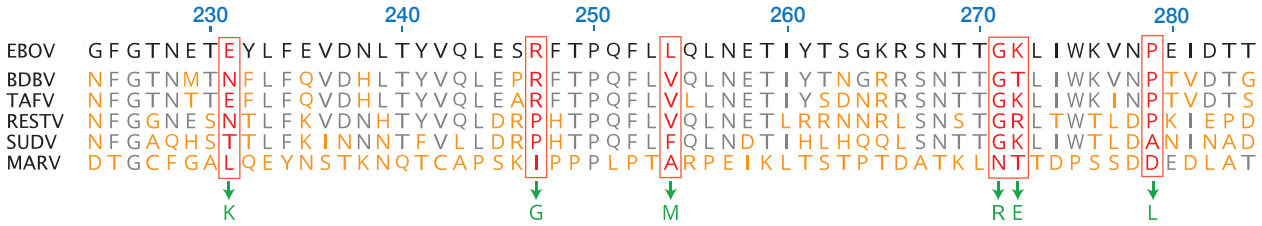

C

ADI-15878 putative epitope + escape mutants (original residue→mutant residue)

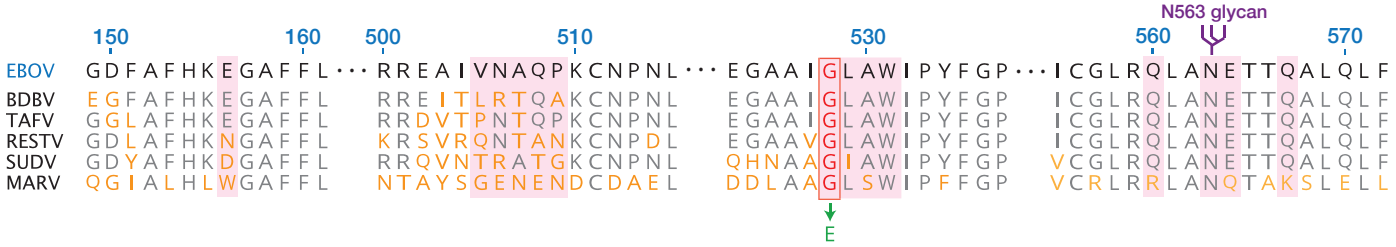

D

ADI-15946 putative epitope + escape mutants (original residue→mutant residue)

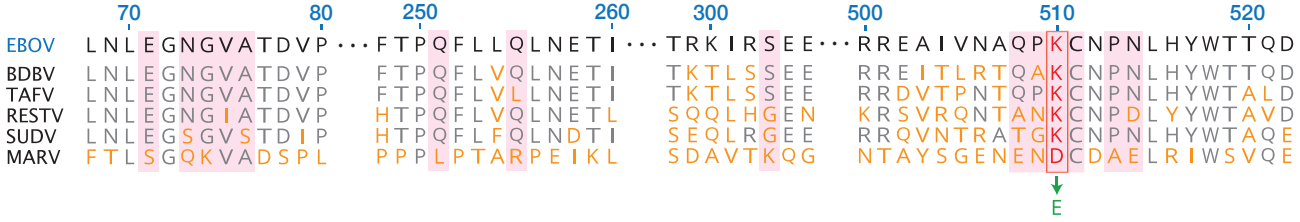

Figure S3. Locations of viral neutralization escape mutations and putative NAb epitopes in filovirus GP, related to Figure 3

(A–D) Amino acid sequence alignments of regions of filovirus GP encompassing each escape mutation and putative NAb epitope are shown (EBOV GP numbering). Gray, conserved residues. Orange, divergent residues. Putative NAb contact residues derived from the EM image reconstructions (Figure 3) are shaded in pink. Positions of escape mutations are boxed and labeled in red, and the residue changes are indicated in green. In panel C, the location of the conserved N–linked glycan at residue 563 is indicated in purple.

Figure S4

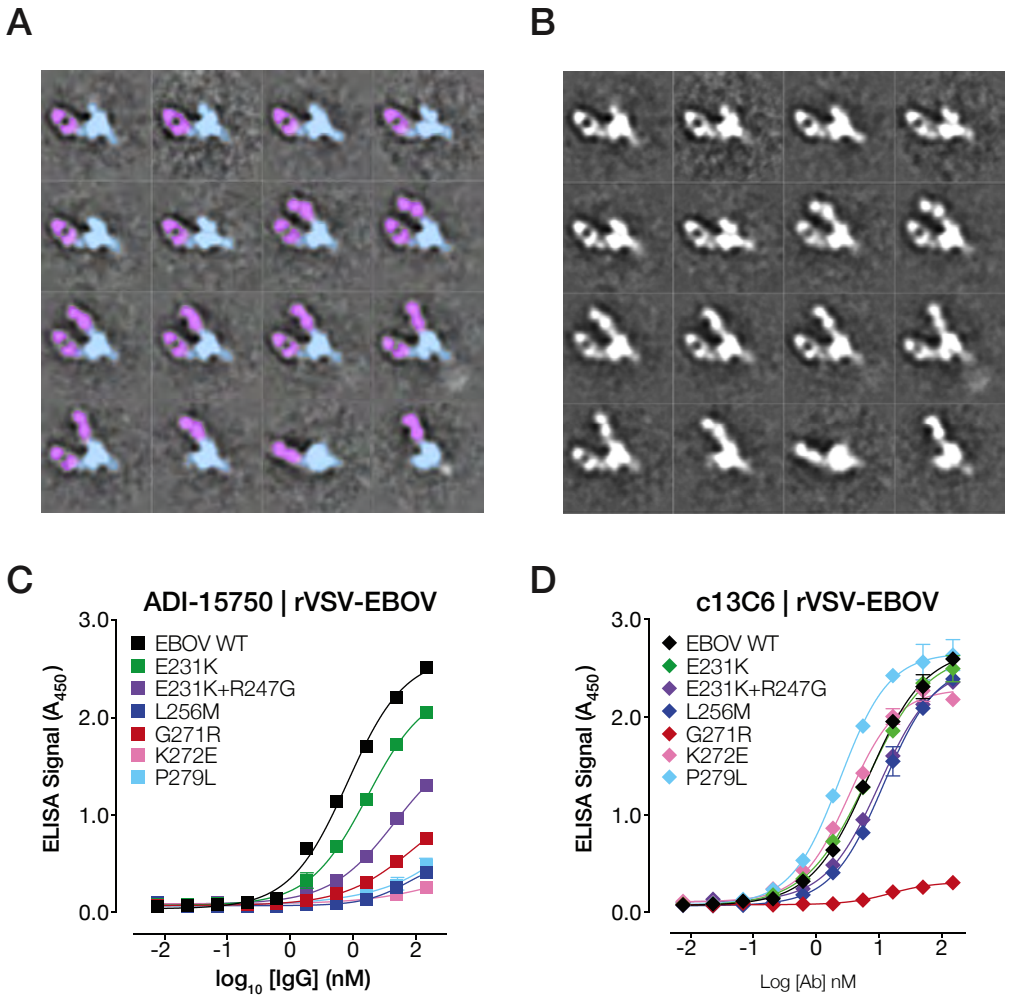
A
B
C
ADI-15750 | rVSV-EBOV
EBOV WT
E231K
E231K+R247G
L256M
G271R
K272E
P279L
ELISA Signal (A450)
3.0
2.0
1.0
0.0
-2
-1
0
0
2
log10 [IgG] (nM)
D
c13C6 | rVSV-EBOV
EBOV WT
E231K
E231K+R247G
L256M
G271R
K272E
P279L
ELISA Signal (A450)
3.0
2.0
1.0
0.0
-2
-1
0
1
2
Log [Ab] nM

Figure S4. Sequence and structural properties of GP recognition by ADI-15750, related to Figure 3

(A–B) 2D class averages of the ADI-15750 FAb:EBOV GPΔTM complex derived by negative-stain EM are shown.

(A) Class averages are pseudocolored to highlight GP (cyan) and Fab (lilac).

(C–D) Capacity of ADI-15750 (C) and the glycan cap binder c13C6 (D) to recognize rVSV-EBOV GPs bearing ADI-15750—neutralization-escape variants in an ELISA. Means±SD for three replicates are shown.

Figure S5

A

Ligand	Analyte	k_{on} (M^{-1} s^{-1})	k_{off} (s^{-1})	K_D (nM)
ADI-15878 (HC^{WT}:LC^{WT})	GP	$(1.90\pm0.01)\times10^{4}$	$<1.0\times10^{-7}$	<0.001
ADI-15878 (HC^{IGL}:LC^{WT})	GP	$(6.90\pm0.07)\times10^{3}$	$(3.1\pm0.4)\times10^{-5}$	4.4±0.6
ADI-15878 (HC^{WT}:LC^{IGL})	GP	$(5.2\pm0.1)\times10^{3}$	$(1.26\pm0.06)\times10^{-4}$	24±1
ADI-15878 (HC^{IGL}:LC^{IGL})	GP	$(4.5\pm0.3)\times10^{3}$	$(1.92\pm0.06)\times10^{-3}$	420±30
ADI-15878 (HC^{WT}:LC^{WT})	GP_{CL}	$(3.01\pm0.01)\times10^{5}$	$<1.0\times10^{-7}$	<0.001
ADI-15878 (HC^{IGL}:LC^{WT})	GP_{CL}	$(3.13\pm0.01)\times10^{5}$	$(1.33\pm0.04)\times10^{-4}$	0.4±0.1
ADI-15878 (HC^{WT}:LC^{IGL})	GP_{CL}	$(3.30\pm0.01)\times10^{5}$	$(8.1\pm0.2)\times10^{-5}$	0.3±0.1
ADI-15878 (HC^{IGL}:LC^{IGL})	GP_{CL}	$(3.02\pm0.01)\times10^{5}$	$(5.6\pm0.1)\times10^{-4}$	2.2±0.1

B

Ligand	Analyte	k_{on} (M^{-1} s^{-1})	k_{off} (s^{-1})	K_D (nM)
ADI-15878 (WT)	GP	$(1.90\pm0.01)\times10^{4}$	$<1.0\times10^{-7}$	<0.001
ADI-15878 (D95A)	GP	$(1.18\pm0.01)\times10^{4}$	$(8.8\pm0.1)\times10^{-4}$	74±1
ADI-15878 (H96A)	GP	$(3.86\pm0.04)\times10^{4}$	$(1.8\pm0.1)\times10^{-4}$	4.5±0.2
ADI-15878 (R97A)	GP	$(2.02\pm0.02)\times10^{4}$	$(1.90\pm0.05)\times10^{-4}$	9.4±0.3
ADI-15878 (V98A)	GP	$(4.66\pm0.03)\times10^{4}$	$(1.85\pm0.05)\times10^{-4}$	4.0±0.1
ADI-15878 (W99A)	GP	$(2.59\pm0.12)\times10^{4}$	$(3.47\pm0.05)\times10^{-3}$	130±6
ADI-15878 ($G100_bA$)	GP	$(1.99\pm0.01)\times10^{4}$	$(5.22\pm0.14)\times10^{-7}$	0.03± 0.01
ADI-15878 ($Y100_cA$)	GP	$(9.4\pm0.3)\times10^{3}$	$(2.78\pm0.05)\times10^{-4}$	30±1
ADI-15878 ($H100_dA$)	GP	$(9.9\pm0.1)\times10^{3}$	$(1.80\pm0.03)\times10^{-4}$	18±0.4
ADI-15878 ($F100_eA$)	GP	$(1.05\pm0.01)\times10^{4}$	$(3.91\pm0.08)\times10^{-4}$	37±1
ADI-15878 (D101A)	GP	$(2.43\pm0.03)\times10^{4}$	$(3.2\pm0.6)\times10^{-5}$	1.3±0.3
ADI-15878 (Y102A)	GP	$(2.23\pm0.02)\times10^{4}$	$(1.32\pm0.06)\times10^{-4}$	5.9±0.3

C

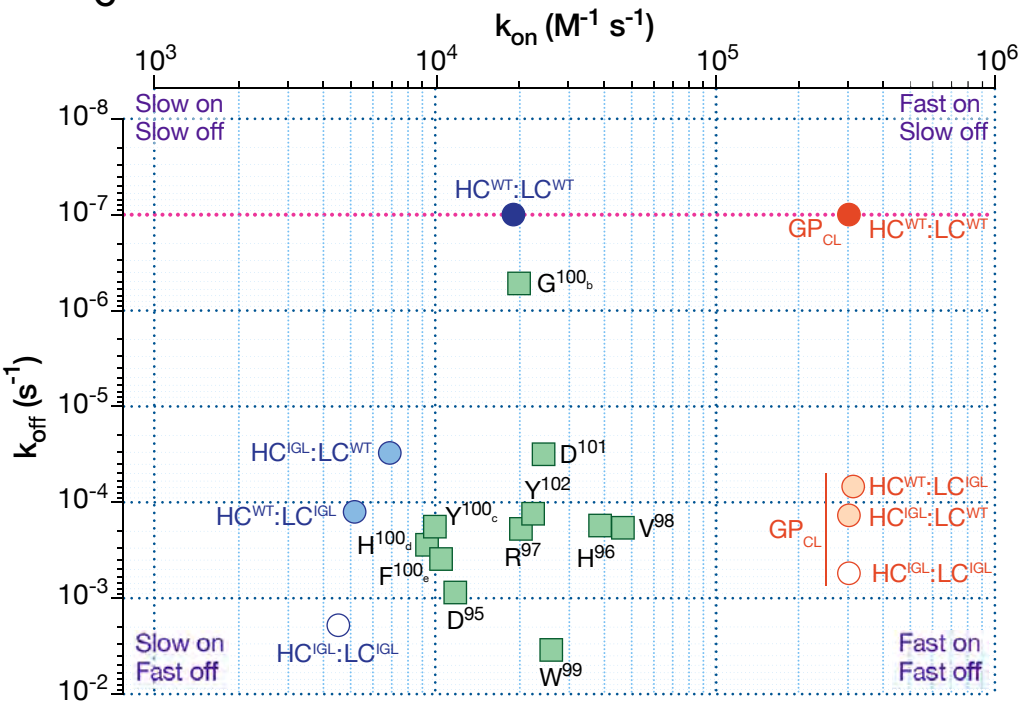

Figure S5. Summary of GP binding properties of ADI-15878 variants, related to Figure 6

(A) Kinetic binding constants for recognition of uncleaved and cleaved EBOV GPΔTM (GP and GP_{CL}, respectively) by WT and inferred germline (IGL) ADI-15878 variants were determined by BLI. HC, mAb heavy chain; LC, mAb light chain. k_{on}, association rate constant; k_{off}, dissociation rate constant; K_D, equilibrium dissociation constant. 95% confidence intervals are reported for each binding constant.

(B) Kinetic binding constants for recognition of EBOV GPΔTM by ADI-15878 bearing the indicated mutations in the CDR-H3 loop were determined by BLI. 95% confidence intervals are reported for each binding constant.

(C) Graphical representation of the association and dissociation rate constants from panels A–B. The lower limit of detection for the dissociation rate constant is shown as a pink line.

Figure S6

A

ADI-15878	EBOV	BDBV	TAFV	SUDV	RESTV
HC^{WT}:LC^{WT}	1.0	0.4	0.9	0.8	0.1
HC^{IGL}:LC^{WT}	5.8	1.8	5.2	30	>400
HC^{WT}:LC^{IGL}	12	1.5	9	nn	nn
HC^{IGL}:LC^{IGL}	nn	nn	nn	nn	nn
HC^{WT}:LC^{WT}	0.01			0.02	
HC^{IGL}:LC^{WT}	0.03			1.7	
HC^{WT}:LC^{IGL}	0.03			20	
HC^{IGL}:LC^{IGL}	200			200	

Neut. IC_{50}: <2 nM, <10 nM, <50 nM, <250 nM, <500 nM, Non-neut. (GP); <0.1 nM, <1 nM, <10 nM, <100 nM, <250 nM, Non-neut. (GP_{CL})

B

CDR-H3	EBOV	BDBV	TAFV	SUDV	RESTV
WT	1.0	0.4	0.9	0.8	0.1
D95A	> 500	nn	> 350	nn	nn
H96A	1.0	0.4	0.8	1.0	0.2
R97A	3.2	0.4	1.9	1.5	0.2
V98A	0.6	0.2	1.0	1.1	0.2
W99A	nn	>200	>150	nn	nn
$G100_bA$	0.8	0.4	0.8	0.9	0.2
$Y100_cA$	3.0	0.8	0.8	> 350	1.3
$H100_dA$	3.2	0.6	2.2	2.1	0.5
$F100_eA$	4.2	0.3	2.8	2.1	0.4
D101A	2.0	0.9	2.1	1.5	0.4
Y102A	0.8	0.4	1.1	0.8	0.1

Neut. IC_{50}: <2 nM, <10 nM, <50 nM, <250 nM, <500 nM, Non-neut.

C

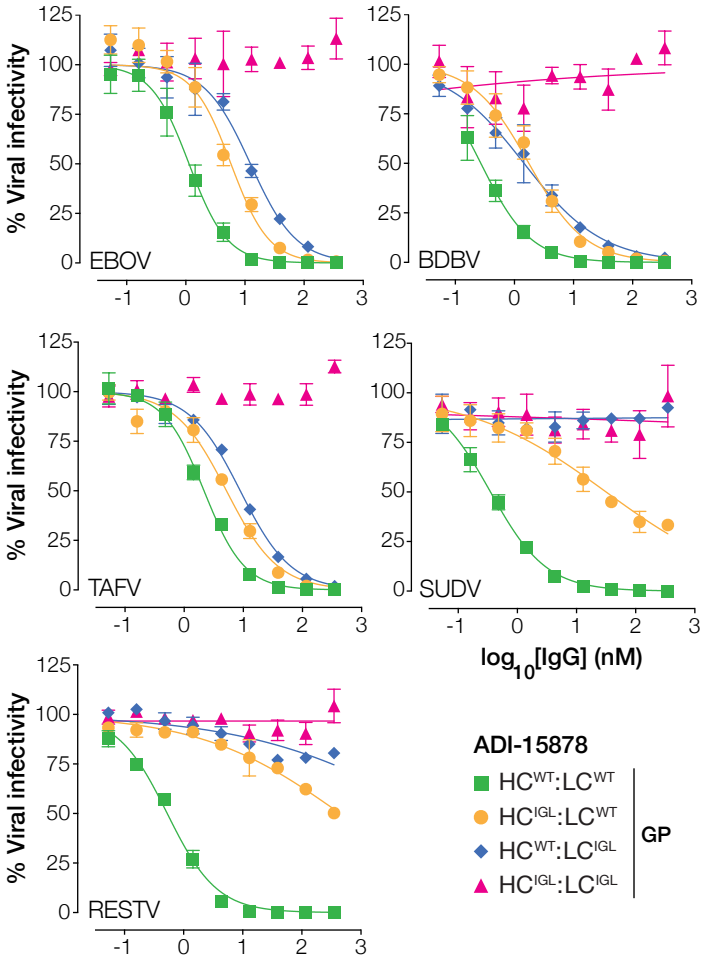

D

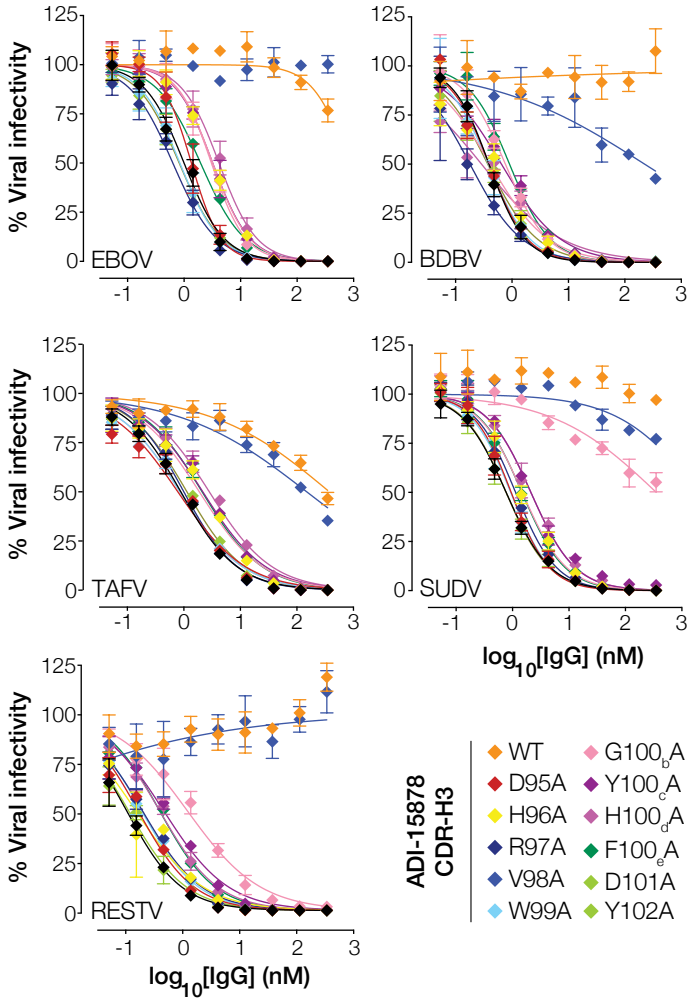

E

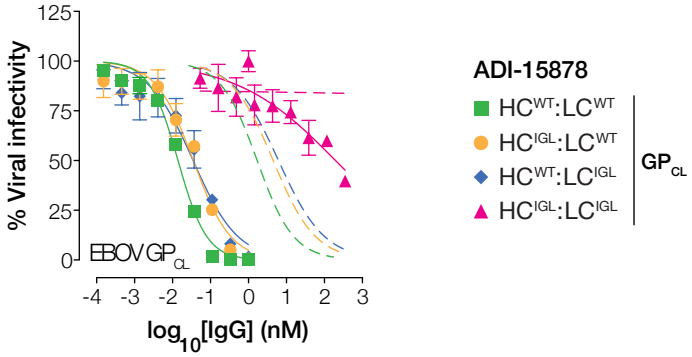

Figure S6. Summary of viral neutralization properties of ADI-15878 variants, related to Figure 6

(A) Heat maps and IC_{50} values for neutralization of rVSVs bearing uncleaved and cleaved ebolavirus GPs by ADI-15878 inferred-germline (IGL) variants. nn, non-neutralizing.

(B) Heat maps and IC_{50} values for neutralization of rVSVs bearing ebolavirus GPs by ADI-15878 bearing the indicated mutations in the CDR-H3 loop.

(C–D) Neutralization dose curves from which data in panels A and B were derived.

(E) Dose curves for neutralization of cleaved rVSV-EBOV GP_{CL} particles by ADI-15878 IGL variants. Corresponding dose curves for uncleaved rVSV-EBOV GP are showed as dashed lines. In panels C–E, means±SD for three replicates are shown.

Table S1

	rVSV-GP neutralization IC_{50} (nM)[a]						
mAb	**EBOV**	**BDBV**	**TAFV**	**SUDV**	**RESTV**	**LLOV**	**MARV**
HR2/Stalk Binding Group[b]							
ADI-16061	0.2	0.6	4.8	–[c]	–	–	–
ADI-15975	5.9	60	20	40	500		
13C6 Competition Group (glycan cap binders)[b]							
ADI-15750	9	–	0.8	34	22	–	–
ADI-15968	12	120	4.1	43	–		
KZ52 Competition Group (base binders)[b]							
ADI-15742	2.0	1.0	1.5	0.5	0.2	–	–
ADI-15878	0.5	0.5	1.0	0.3	0.2	–	–
ADI-15881	30	70	–	60	–		
ADI-15887	9	12	–	230	230		
ADI-15946	2.5	0.4	8	40	–	–	–
ADI-16047	9	160	500	150	90		

Table S1. Summary of rVSV-GP neutralization by cross-neutralizing human mAbs, related to Figure 1

[a]IC_{50}, mAb concentration that affords half-maximal neutralization of viral infectivity.
[b]mAbs were binned by competition/epitope group. See Figure 3 and text for details.
[c]No detectable neutralizing activity

Table S2

Authentic virus neutralization IC_{50} (nM)[a]			
mAb	EBOV	BDBV	SUDV
HR2/Stalk Binding Group			
ADI-16061	0.1	0.3	300
13C6 Competition Group (glycan cap binders)			
ADI-15750	5.2	–	–
KZ52 Competition Group (base binders)			
ADI-15742	0.7	0.6	0.2
ADI-15878	0.2	0.6	0.2
ADI-15946	0.6	1.5	120

Table S2. Summary of authentic ebolavirus neutralization by cross-neutralizing human mAbs, related to Figure 2

Table S3

Ligand	Analyte	pH	k_{on} (M^{-1} s^{-1})	k_{off} (s^{-1})	K_D (nM)
KZ52	GP	7.5	$(4.73\pm0.04)\times10^{4}$	$(2.92\pm0.03)\times10^{-4}$	6.2±0.8
KZ52	GP	5.5	$(1.40\pm0.04)\times10^{4}$	$(4.35\pm0.03)\times10^{-4}$	31±1
KZ52	GP_{CL}	5.5	$(1.48\pm0.02)\times10^{5}$	$(5\pm1)\times10^{-5}$	0.4±0.1
c2G4	GP	7.5	$(4.61\pm0.05)\times10^{4}$	$(5.53\pm0.03)\times10^{-4}$	12.0±0.1
c2G4	GP	5.5	$(3.2\pm0.5)\times10^{3}$	$(6.16\pm0.04)\times10^{-4}$	190±30
c2G4	GP_{CL}	5.5	$(2.91\pm0.02)\times10^{5}$	$(1.78\pm0.08)\times10^{-4}$	6.2±0.1
c4G7	GP	7.5	$(1.82\pm0.02)\times10^{5}$	$(4.08\pm0.04)\times10^{-4}$	2.2±0.1
c4G7	GP	5.5	$(1.90\pm0.06)\times10^{4}$	$(4.33\pm0.04)\times10^{-4}$	23±1
c4G7	GP_{CL}	5.5	$(4.34\pm0.02)\times10^{5}$	$(7.1\pm0.4)\times10^{-5}$	0.16±0.01
ADI-15946	GP	7.5	$(3.69\pm0.04)\times10^{4}$	$(3.15\pm0.02)\times10^{-4}$	8.5±0.1
ADI-15946	GP	5.5	$(1.52\pm0.01)\times10^{5}$	$(3.60\pm0.02)\times10^{-4}$	2.4±0.02
ADI-15946	GP_{CL}	5.5	$(4.48\pm0.02)\times10^{5}$	$<1\times10^{-7}$ [a]	<0.001[a]
ADI-18578	GP	7.5	$(5.22\pm0.04)\times10^{4}$	$<1\times10^{-7}$ [a]	<0.001[a]
ADI-18578	GP	5.5	$(4.35\pm0.04)\times10^{4}$	$(1.50\pm0.02)\times10^{-4}$	3.4±0.1
ADI-18578	GP_{CL}	5.5	$(3.0\pm0.1)\times10^{5}$	$<1\times10^{-7}$ [a]	<0.001[a]

Table S3. Kinetic binding constants for recognition of uncleaved and cleaved EBOV GP by human and mouse base-binding NAbs determined by BLI, related to Figure 5.
[a]Dissociation rate constants (k_{off}) and equilibrium dissociation constant (K_D) values for these mAbs represent lower estimates.